Peripheral Facial Nerve Axotomy in Mice Causes Sprouting of Motor Axons Into Perineuronal Central White Matter: Time Course and Molecular Characterization

Milan Makwana,[1] Alexander Werner,[2,3] Alejandro Acosta-Saltos,[1] Roman Gonitel,[1,4] Abirami Pararajasingham,[1] Crystal Ruff,[1] Prakasham Rumajogee,[1] Dan Cuthill,[1] Mathias Galiano,[1,2] Marion Bohatschek,[1] Adam S. Wallace,[1] Patrick N. Anderson,[5] Ulrike Mayer,[6] Axel Behrens,[7] and Gennadij Raivich[1,2,5]*

[1]Perinatal Brain Repair Group, Department of Obstetrics and Gynaecology, EGA Institute for Women's Health, University College London, London WC1E 6HX, United Kingdom
[2]Department of Neuromorphology, Max-Planck Institute for Neurobiology, 82152 Martinsried, Germany
[3]Aurigon Co., D-82327 Tutzing, Germany
[4]Molecular Immunology Unit, Institute of Child Health, University College London, London WC1E 6HX, United Kingdom
[5]Department of Anatomy and Developmental Biology, University College London, London WC1E 6HX, United Kingdom
[6]Biomedical Research Centre, University of East Anglia, Norwich NR4 7, United Kingdom
[7]Cancer Research UK, London Research Institute, London WC2A 3PX, United Kingdom

ABSTRACT

Generation of new axonal sprouts plays an important role in neural repair. In the current study, we examined the appearance, composition and effects of gene deletions on intrabrainstem sprouts following peripheral facial nerve axotomy. Axotomy was followed by the appearance of galanin$^+$ and calcitonin gene-related peptide (CGRP)$^+$ sprouts peaking at day 14, matching both large, neuropeptide$^+$ subpopulations of axotomized facial motoneurons, but with CGRP$^+$ sprouts considerably rarer. Strong immunoreactivity for vesicular acetylcholine transporter (VAChT) and retrogradely transported MiniRuby following its application on freshly cut proximal facial nerve stump confirmed their axotomized motoneuron origin; the sprouts expressed CD44 and alpha7beta1 integrin adhesion molecules and grew apparently unhindered along neighboring central white matter tracts. Quantification of the galanin$^+$ sprouts revealed a stronger response following cut compared with crush (day 7–14) as well as enhanced sprouting after recut (day 8 + 6 vs. 14; 14 + 8 vs. 22), arguing against delayed appearance of sprouting being the result of the initial phase of reinnervation. Sprouting was strongly diminished in brain Jun-deficient mice but enhanced in alpha7 null animals that showed apparently compensatory up-regulation in beta1, suggesting important regulatory roles for transcription factors and the sprout-associated adhesion molecules. Analysis of inflammatory stimuli revealed a 50% reduction 12–48 hours following systemic endotoxin associated with neural inflammation and a tendency toward more sprouts in TNFR1/2 null mutants (P = 10%) with a reduced inflammatory response, indicating detrimental effects of excessive inflammation. Moreover, the study points to the usefulness of the facial axotomy model in exploring physiological and molecular stimuli regulating central sprouting. J. Comp. Neurol. 518:699–721, 2010.

INDEXING TERMS: growth cones; regeneration; central sprouting; adhesion molecules; transcription factors; inflammation

Additional Supporting Information may be found in the online version of this article.

The first three authors contributed equally to this work.

Grant sponsor: International Spinal Research Trust Natalie-Rose-Barr Fellowship (to M.M., G.R.); Grant sponsor: Motor Neuron Disease (MND) Association; Grant number: 06/6220 (to A.A.-S., G.R.); Grant sponsor: Biotechnology and Biological Sciences Research Council; Grant number: 31/S20299 (to G.R.); Grant number: BB/D009537/1 (to G.R.).

*CORRESPONDENCE TO: Gennadij Raivich, MD, PhD, Perinatal Brain Repair Group, Department of Obstetrics and Gynaecology and Department of Anatomy and Developmental Biology, University College London, 86-96 Chenies Mews, London WC1E 6HX, United Kingdom. E-mail: g.raivich@ucl.ac.uk

Received 2 June 2008; Revised 18 June 2009; Accepted 2 October 2009.
DOI 10.1002/cne.22240
Published online October 13, 2009 in Wiley InterScience (www.interscience.wiley.com).

Generation of new axonal sprouts and the process of axonal elongation play a vital role in the neural repair program following injury to the nervous system. In the classical case of axonal regeneration in the injured peripheral nerve, the tip of the proximal axon still connected to the neuronal cell body is gradually transformed into a motile and sprouting growth cone that moves across the gap between the proximal and nerve stump, enters neural tubes in the distal part, and uses them as a scaffold on its way to the peripheral target (Witzel et al., 2005). Supernumerary axonal sprouts can also develop more proximally, at the nodes of Ranvier (Ramon y Cajal, 1928; Friede and Bischausen, 1980; McQuarrie, 1985; Ide and Kato, 1990), from distal dendrites (Fenrich et al., 2007), and occasionally even at the level of the injured neuronal cell body (Linda et al., 1985).

In addition to outright regeneration, nerve injury can also elicit sprouting from uninjured axons. This includes collateral sprouting from functionally appropriate or inappropriate adjacent intact axons into the deafferented part of the central nervous system (Cotman et al., 1990) or peripheral tissues, including skin (Diamond et al., 1987), muscle (Mehta et al., 1993; Nguyen et al., 2002), and nerve (Ide and Kato, 1990; Tanigawa et al., 2005). Peripheral axotomy can also induce the sprouting of central sensory processes of the affected dorsal root ganglia (DRG) neurons in the spinal cord (Woolf et al., 1992) as well as the appearance of perineuronal neurite baskets in the DRGs themselves (McLachlan et al., 1993; McLachlan and Hu, 1998; Li and Zhou, 2001; Liu et al., 2005). Both processes have been indcated to contribute to posttraumatic neuropathic pain (Woolf et al., 1992; Liu et al., 2005). Despite the variability in origin, regulation, and dynamics, in most cases these different forms of posttraumatic neurite outgrowth appear to start within the first few days after injury or to represent a very late response that may be associated with frustrated regeneration.

Transection of the adult facial nerve is a well-established model system for studying the axonal response and neuronal regeneration (Moran and Graeber, 2004). Moreover, experimental work in gene-deficient and-overexpressing mice has begun to provide insight into molecular signals—transcription factors, cell adhesion molecules, cytokines, and neurotrophins—that determine axonal regeneration as well as posttraumatic neuronal survival and cell death and different aspects of the neural inflammatory response (Werner et al., 2000; Kalla et al., 2001; Heumann et al., 2001; Raivich et al., 2004; for review see Raivich and Makwana, 2007). However, these studies also suggested a de novo appearance of neuropeptide-immunoreactive sprouts in and around the axotomized facial motor nucleus, during the midphase of axonal regeneration after facial nerve cut (Kloss et al., 1999; Werner et al., 2000; Galiano et al., 2001).

The aim of the current study was to determine the precise neuronal origin of these sprouting neurites and define their time course, neuroanatomical distribution, and molecular characteristics. We show that these axons originate from injured and regenerating neurons, are capable of growing for more than 0.5 mm into different white matter tracts surrounding the lesioned facial motor nucleus, and express high levels of cell adhesion molecules such as CD44 and alpha7beta1 integrin. Surprisingly, deletion of the alpha7 integrin subunit led to a further increase in the number and extent of neuropeptide-immunoreactive neurite growth cones, suggesting an inhibitory role of alpha7 in this form of posttraumatic central axonal sprouting.

MATERIALS AND METHODS

Animals, surgical procedures, and tissue treatment

Normal, wild-type, C57Bl/6 mice were generated at our animal facilities at Max-Planck Institute of Neurobiology, Martinsried, and then at the Biological Services Unit, UCL. Transgenic, TNFR1/2−/− mice and wild-type controls (+/+) were obtained from BRL (Basel, Switzerland) and were on a mixed B6 × 129 background. In the TNFR1 transgenic strain, TNFR1 gene exons II and III, flanked by the Nhe I and Bgl II restriction sites were replaced by ortho-oriented pgk-neomycin resistance cassette, abolishing specific tumor necrosis factor-α (TNFα) binding in TNFR1−/− thymocytes (Rothe et al., 1993). In the TNFR2 strain, the pgk-neomycin resistance cassette was inserted into the BstB II site of the second TNFR2 exon, just downstream of the sequence encoding the signal peptide, resulting in a complete lack of TNFR2 protein (Erickson et al., 1994). Both strains were crossed together, to obtain double heterozygotes (TFR1+/−TNFR2+/−), then crossed again for the TNFR1&2−/− and controls.

Brain c-Jun-deficient animals were generated by crossing mice carrying a floxed *jun* allele encoding c-Jun, jun^{f}, with the loxP sequences at the XbaI restriction sites surrounding the exon carrying the entire c-Jun open reading frame (Behrens et al., 2002), with those expressing cre recombinase under the control of nestin promoter nes::cre. In the nes::cre transgene, the cre gene is placed immediately downstream of the 5-kb large 5′-promoter, followed by the human growth hormone polyadenylation signal and the second nestin intron, which contains a neuroepithelium-specific enhancer (Tronche et al., 1999). The resulting $jun^{f/wt}$ × nestin::cre animals were then crossed again with $jun^{f/f}$, to generate the $jun^{f/f}$ × nestin::cre mutant mice, in which both *jun* alleles are inactivated in cells derived from embryonic neuroepithelium

($jun^{\Delta n}$). Compound $jun^{\Delta n}$ mice were on a mixed 129Ola/C57BL6/FVBN genetic background. Sibling animals lacking the cre transgene, with functional, unrecombined homozygous jun^{f} ($jun^{f/f}$), served as controls. The homozygous alpha7−/−and littermate controls on the 129/Sv background used in this study were obtained from heterozygous crossing of alpha7+/−mice generated by Mayer et al. (1997). In that transgenic strain, a 1-kb stretch of the alpha7 genomic sequence flanked by the NcoI restriction sites including part of exon 1 and the following intron and encoding the entire signal sequence plus 107 bases coding for the start part of the mature protein is replaced by a reverse-oriented neomycin resistance cassette (Mayer et al., 1997).

To study the effects of enhanced neural inflammation, *Escherichia coli* lipopolysaccharide (O55:B5 serotype, 1 mg; Sigma, Deisenhofen, Germany) was dissolved in phosphate-buffered saline (PBS: 10 mM Na_2HPO_4, 0.85% NaCl, pH 7.4), and injected intraperitoneally into C57 black 6 mice (8 weeks old, 25–30 g weight; n = 3 per group) 12–96 hours prior to the 14-day time point. Control groups of animals were left alone or were injected with saline and allowed to survive for 24 hours.

All surgical techniques were performed with animals under anesthesia with 2,2,2-tribromethanol (Avertin; Sigma, Deisenhofen, Germany), 0.4 mg/g body weight, on 3–6-month-old mice. All animals belonging to the same experimental group (day 1 group, day 2 group, day 4 group, etc.) were also operated upon on the same day, inside a narrow time window of 1–3 hours. Animal experiments and care protocols were approved by the Regierung von Oberbayern (AZ 211-2531-10/93 and AZ 211-2531-37/97) in Germany and the Home Office (Scientific Procedures Act) in the United Kingdom.

The right facial nerve (including the retroauricular branch) was cut or crushed at its exit from the stylomastoid foramen. For the reaxotomy experiments, the cut was made 1 mm distal to the original injury, and the retroauricular branch was not recut. Animals were euthanized after survival times of 1–42 days and perfusion fixed with 200 ml PBS (10 mM Na_2HPO_4, 0.85% NaCl, pH 7.4), followed by 200 ml of 4% paraformaldehyde in PBS (PFA/PBS), then by a 2-hour immersion of the brainstem in 1% PFA/PBS at 4°C on a rotator (8 rpm), with an overnight rotating immersion in a phosphate-buffered sucrose solution (PB: 10 mM Na_2HPO_4, pH 7.4, 4°C; 30% sucrose), and frozen on dry ice.

Immunofluorescence, double labeling, and confocal scanning microscopy

Frozen brainstems were cut at the level of the facial nucleus, and 20-μm sections were collected on warm, 0.5% gelatin-coated slides (Merck, Darmstadt, Germany), refrozen on dry ice, and stored at −80°C until further use. Axonal growth cones in and around the facial motor nuclei were quantified by using immunofluorescence against CGRP or galanin, the neuropeptides expressed in axotomized facial motoneurons. For standard immunofluorescence, the sections were thawed, rehydrated and spread in distilled water, fixed in 4% formaldehyde in 0.1 M PB, defatted in acetone, and pretreated with 5% goat serum (Vector, Wiesbaden, Germany) in phosphate buffer/PB as described by Möller et al. (1996). Briefly, the sections were incubated overnight at 4°C with 1:100 diluted, primary rabbit antibodies against CGRP or galanin (Table 1), washed in PB, and incubated with a biotinylated goat anti-rabbit antibody (1:100; Vector) and Texas red streptavidin (Jackson Laboratories). The sections were then covered with VectaShield (Vector) and stored in the dark at 4°C for confocal scanning and quantification.

For immunofluorescence, fixed sections were preincubated as in brightfield immunohistochemistry. Both primary antibodies were applied overnight at 4°C, washed, incubated with two appropriate secondary antibodies (biotin-conjugated donkey anti-rabbit Ig and FITC-conjugated goat anti-rat Ig; 1:100; Dianova, Hamburg, Germany), washed again, and then incubated with a tertiary FITC-conjugated donkey anti-goat antibody (1:100; Sigma) and Cy3-avidin (1:1,000; Dianova). In the case of colocalization with the goat anti-VAChT, only the donkey anti-goat antibody was used. Omission of the primary antibody or replacement with nonspecific immunoglobulin from the same species (rat, rabbit, or hamster) at the same dilution led to the disappearance of specific labeling.

Digital micrographs of FITC and Cy3 or Texas red fluorescence were taken with a Leica TCS confocal laser microscope with a ×10 objective for quantification and a ×100 objective for illustrations in eight-bit gray-scale, 1,024 × 1,024 pixel format as described in previous studies (Raivich et al., 1998; Kloss et al., 1999). Twelve consecutive equidistant levels with 30-μm spacing with a ×10 objective or 20 levels with 0.5-μm spacing at ×100 objective were recorded and condensed onto a single bitmap by using the MaxIntense algorithm.

Antibody characterization

A summary of primary, secondary, and tertiary antibodies used to characterize the facial sprouts by double labeling with antibodies for galanin, CGRP, or vesicular acetylcholine transporter (VAChT) 14 days after facial nerve cut are listed in Table 1. The specificity of alpha7, alphaM, CD44, CGRP, and galanin was confirmed by using the appropriate knockouts, compared with the wild-type controls. Homozygous deletion of the alpha7 gene caused the disappearance of neuronal and terminal alpha7 immunoreactivity in facial motoneurons as well as throughout the

TABLE 1.
Summary of Antibodies[1]

Detected antigen	Immunization with	Primary antibody (code, type)	Dilution	Application	Source
Alpha4 integrin (CD49d)	Mouse spontaneous T-lymphoma line TK1 (AKR Cum strain)	R1-2, 01271D, RtM, IgG2b, κ	1:1,000	DIF	Pharmingen, United Kingdom catalog No. 553154 lot No. 38618
Alpha5 integrin (CD49e)	Mouse mast cell line MC/9	5H10-27 (MFR5) RtM, IgG2a, κ	1:200	DIF	Pharmingen, United Kingdom catalog No. 553319 lot No. C510514
Alpha6 integrin (CD49f)	Mouse mammary tumour (balb/C)	GoH3, RtM, IgG2a	1:3,000	DIF	Serotec, United Kingdom catalog No. MCA699GA
Alpha7 integrin (CD49g)	Synthetic peptide (aa 1117-1136) coupled to maleimide-activated key limphole hemocyanin (KLH), Pierce, Rockford, IL	Anti-alpha7, RbP	1:5,000	IHC, DIF	Ulrike Meyer, U East Anglia Norwich, United Kingdom
AlphaM integrin (CD11b)	T-cell-enriched B10 mouse spleen cells	5C6, RtM	1:6,000	DIF	Serotec, United Kingdom catalog No. MCA 711
Beta1 integrin (CD29)	Raised against the beta1 integrin (von Ballestrem et al., 1996)	MB1.2, RtM, IgG2a, κ	1:3,000	IHC, DIF	Chemicon, United Kingdom catalog No. MAB1997 lot No. 0507004326
CD44	Purified human blood lymphocyte CD44 lacking v1–v10 exons	MAB2137, RtM, IgG2b	1:5,000	DIF	Chemicon, United Kingdom catalog No. MAB2137
CGRP	Calcitonin gene-related peptide (Bachem)[2]	anti-CGRP, RbP	1:400	IHC, DIF	Bachem, United Kingdom T-4032.0050
Galanin	Galanin peptide (Bachem)[3]	Antigalanin, RbP	1:400	IHC, DIF	Bachem, United Kingdom T-4334.0050
MAP2	Purified rat brain microtubule-associated protein (MAP2)	Anti-MAP2, RbP, AB5622	1:3,000	DIF	Chemicon, United Kingdom P11137 AB5622
NF-H	Rat NFH fusion protein containing 37 KSP repeats	anti-NFH, RbP AB1991	1:200	DIF	Chemicon, United Kingdom catalog No. AB1991 lot No. 23080338
VaChT	Synthetic peptide (aa 511-530) from the cloned rat VAChT	G4481, GtP AB1588	1:6,000	DIF	Chemicon, United Kingdom AB1588
Secondary and tertiary					
Goat Ig	Goat immunoglobulin	FITC-cj α-Gt Ig, DkP	1:100	DIF	Dianova, United Kingdom
Hamster Ig	Hamster immunoglobulin	FITC-cj α-Hm Ig, GtP	1:100	DIF	Dianova, United Kingdom
Rat Ig	Rat immunoglobulin	Biot. α-Rt Ig, GtP	1:100	IHC	Vector, United Kingdom
Rat Ig	Rat immunoglobulin	FITC-cj α-Rt Ig, GtP	1:100	DIF	Dianova, United Kingdom
Rabbit Ig	Rabbit immunoglobulin	Biot α-Rb Ig, GtP	1:100	IHC	Vector, United Kingdom
Rabbit Ig	Rabbit immunoglobulin	Biot α-Rb Ig, DkP	1:100	DIF	Dianova, United Kingdom

[1]Antigens: CD44, cluster of differentiation 44; CGRP, calcitonin gene-related peptide; MAP2, microtubule-associated protein 2; NFHm, neurofilament heavy isoform; VaChT, vesicular acetylcholine transporter. Antibodies: RtM, rat monoclonal; HmM, hamster monoclonal; RbP, rabbit polyclonal; GtP, goat polyclonal; DkP, donkey polyclonal; FITC-cj fluorescein isothiocyanate conjugated. Applications: DIF, double immunofluorescence; IHC, immunohistochemistry (light microscopy).

[2]CGRP peptide sequence: H-Ser-Cys-Asn-Thr-Ala-Thr-Cys-Val-Thr-His-Arg-Leu-Ala-Gly-Leu-Leu-Ser-Arg-Ser-Gly-Gly-Val-Val-Lys-Asp-Asn-Phe-Val-Pro-Thr-Asn-Val-Gly-Ser-Glu-Ala-Phe-NH2, Cys1-Cys2 disulfide bond.

[3]Galanin peptide sequence: H-Gly-Trp-Thr-Leu-Asn-Ser-Ala-Gly-Tyr-Leu-Leu-Gly-Pro-His-Ala-Ile-Asp-Asn-His-Arg-Ser-Phe-Ser-Asp-Lys-His-Gly-Leu-Thr-NH2.

brain and peripheral nerve described in a previous study (Werner et al., 2000). Homozygous alphaM null mice and littermate controls (Hu et al., 2000), obtained through collaboration with Dr Tanya Mayadas Norton (Boston, MA), showed the disappearance of all microglial alphaM immunoreactivity throughout the brain of the alphaM null mice as well as in the axotomized facial motor nucleus. Similar absence of neuronal immunoreactivity for galanin was observed in galanin gene-deficient mice, obtained through collaboration with Dr David Wynick (Holmes et al., 2000); for CGRP in facial motoneurons of the alpha CGRP-deficient mice, through collaboration with Dr Jean-Pierre Changeux (Salmon et al., 2001); and for CD44 in CD44 null mice, provided through collaboration with Dr Rudolf Schmits (Schmits et al., 1997). In all cases, the wild-type littermate controls showed normal, specific immunoreactivity. The null mutants showed very little, diffuse staining throughout the brain.

In addition, antibody specificity for cell adhesion, neuropeptide, and cholinergic markers was further confirmed by Western blotting with unfractionated tissue homogenates from trigeminal ganglia, brainstem, spleen, and

heart muscle. The monoclonal R1-2 antibody against the alpha4 integrin subunit detected a prominent band that migrates at ~80 kDa and a faint band that migrates at ~65 kDa. Although the predicted molecular weight of alpha4 is 115 kDa (UniProt, Q00651), experimentally it has been demonstrated that the molecule is cleaved into fragments of 80 and 66 kDa upon T-cell activation (Blue et al., 1992). The monoclonal 5H10-27 (MFR5) antibody against the alpha5 integrin subunit detected a band at 90 kDa corresponding to the heavy chain. The full predicted molecular weight is 115 kDa; however, it is cleaved into heavy (~90 kDa) and light (~16 kDa) chains, (UniProt, P11688). Cleavage had also been reported experimentally (Teixido et al., 1992) with the products migrating at 80 and 70 kDa under nonreducing conditions. Under reducing conditions, migration of bands might be altered. The monoclonal GoH3 antibody to alpha6 detected a band at 87 kDa corresponding to the heavy chain predicted at 88 kDa (UniProt, Q61739) and a smaller band that migrates at 60 kDa. Cleavage has been previously reported for this molecule with the product migrating at ~70 kDa under nonreducing conditions (King et al., 2008). The polyclonal antibody against alpha7 detected a unique band at 129 kDa corresponding to the full-sized molecule (UniProt, Q61738; Echtermeyer et al., 1996); the monoclonal 5C6 antibody against alphaM detected a single band at 127 kDa corresponding to the full-size molecule (UniProt, P05555). The monoclonal MB1.2 antibody against beta1 detected a band at 88 kDa consistent with the predicted weight (UniProt, P09055) and two smaller bands at 70 and 53 kDa consistent with previously reported cleavage products (Menon et al., 2006). As a general trend, the literature associates proteolytic cleavage of integrins with more active cells. Antibody to CD44 detected a unique band at 63 kDa consistent with the common hematopoetic isoform 6 (UniProt, P15379-5). The polyclonal VAChT antibody detected a single band at 57 kDa as previously reported (UniProt, O35304, http://www.millipore.com/catalogue/item/ab1588). The antibody reveals strong staining on cholinergic terminals surrounding the brainstem and spinal motor neurons as well as comparatively week labeling of the cholinergic neuronal cell body itself (Gilmor et al., 1996). Both features were also confirmed in the current study (see Fig. 5AI–AIK). Galanin antibody detected a single band at 13 kDa consistent with its predicted size (UniProt, P47212). CGRP antibody detected a band at 14 kDa consistent with the signalling peptide (Uniprot, Q99JA0). The Western blots for alpha4, alpha6, alpha7, and beta1 integrin subunits and CD44 in trigeminal ganglion are shown in Supporting Information Figure 3.

The antibodies against microtubule-associated protein 2 (MAP2) and heavy neurofilament isoform (NF-H) were used as previously well-established cellular/subcellular markers. For the anti-MAP2 polyclonal antibody (http://www.millipore.com/catalogue/item/ab5622#), Western blotting with adult rat brain soluble extract detected a strong and specific band for the 280–300-kDa dimer, in our current study, appropriately diluted antibody also resulted in strong dendritic staining, in line with many previous publications (see, e.g., Sigurjonsson et al., 2005; Nateri et al., 2007). For the antineurofilament H (heavy, 200 kDa NFH) polyclonal antibody (http://www.millipore.com/catalogue/item/ab1991#), raised against the rat NFH fusion protein containing 37 lysine-serine-proline (KSP) domain repeats, the manufacturer's data sheet describes strong reactivity to this major neurofilament protein. Insofar as the middle neurofilament protein (160 kDa NFM) also contains a few lysine-serine-proline sequences, there is generally some NFM cross-reactivity, but not with the light 70-kD neurofilament, NFL (Harris et al., 1991). The NFL staining is generally restricted to neurofilaments in the white matter axons (see, e.g., Fig. 5J–L) as well as dendritic and perikaryal neurofilaments in the gray matter.

In the case of rat monoclonal antibodies raised against alpha4 (CD49d), alpha5 (CD49e), alpha6 (CD49f), and beta1 (CD29) integrins, previous studies have also detailed a massive up-regulation of encoding mRNA species following axotomy in the mouse facial motor nucleus, corresponding to a strong increase in the appropriate immunoreactivity (Kloss et al., 1999; Werner et al., 2000). All four monoclonal antibodies are well defined, with long-established functional characterization for alpha4 (Holzmann and Weissman, 1989), alpha5 (Uhlenkott et al., 1996), alpha6 (Hemler et al., 1988), and beta1 (von Ballestrem et al., 1996) integrin subunits. In the mouse, immunoreactivities for all four subunits were colocalized on blood vessel endothelia as well as on activated microglial cells (Hristova et al., 2009), but only the beta1 was also present in axotomized and regenerating motoneurons (Kloss et al., 1999; Raivich et al., 2004). This pattern of just vascular and microglial, and not neuronal (or sprout), immunoreactivity for alpha4, alpha5, and alpha6 immunoreactivity was also reproduced in the current study. The cranial motoneuron expression of the alpha7 and beta1 integrin subunits was also confirmed by Pinkstaff et al. (1999) for trigeminal, facial, and hypoglossal motoneurons.

Quantification of central axonal sprouting

Quantification of growth cones was performed on four sections per facial nucleus, with an interval of 200 μm between each section. Briefly, the sections were scanned in a TCS 4D confocal laser microscope (Leica, Nussloch, Germany) with a ×10 objective using Cy5 settings (ex wavelength 647 nm, LP665, pinhole 30). Fourteen consec-

utive, equidistant levels were recorded and condensed with the MaxIntense projection.

Small, strongly fluorescent growth cones were differentiated from the large neuronal cell bodies with the Sobel filter and a three-step Growth Cone Detection (GCD) algorithm in Optimas 6.2 software (Media Cybernetics, United Kingdom). In the first step, the mean value of the overall luminosity (MEANcor) and the standard deviation (SDcor) of the corrected images (normal image) was recorded. This procedure was repeated following Sobel filter treatment (MEANsob, SDsob, sobel image), which calculates the direction-independent local intensity gradient in a 3×3 pixel kernel. The threshold for neuropeptide-immunofluorescent growth cones in the Sobel image was set with the formula: Threshold = MEANsob + $11 \times$ SDcor. Areas at and above threshold were filtered with the Object Classes function using two additional criteria in the normal image: Area size $>$ 10 pixel and MEANarea –SDarea $>$ $1.4 \times$ MEANcor, with MEANarea being the mean intensity and SDarea the standard deviation for each individual area profile. The remaining areas matched with the profiles of the neuropeptide-immunofluorescent neuronal growth cones and served as a measure for their total area in the tissue section.

In addition, the number of sprouts in and around facial motor nucleus was visually counted by a blinded observer, with the identifying marking on the glass slide covered by an opaque adhesive sticker carrying a code. In this case, two sections per facial nucleus, 320 μm apart, were used to assess the number of sprouts per animal.

Immunohistochemistry for light and electron microscopy

Immunohistochemistry for light microscopy was performed by using the same procedure as for immunofluorescence up to the secondary antibody, followed by incubation with the ABC reagent (Vector), visualization with diaminobenzidine/H_2O_2 (DAB; Sigma, Deisenhofen, Germany), dehydration in alcohol and xylene, and then mounting with Depex (BDH, Poole, United Kingdom). For electron microscopy, 80-μm-thick vibratome sections cut at the facial nucleus level were stained for alpha7 integrin subunit, galanin, or VAChT with a slightly modified protocol (Werner et al., 2000). The vibratome sections were floated; treatment with acetone was omitted; preincubation with goat serum (or donkey serum in case of VAChT) was extended to 4 hours at RT; the rabbit anti-mouse alpha7 antibody was applied at a concentration of 1:500, galanin antibody at 1:400, or VAChT antibody at 1.1,000, overnight; the biotinylated goat anti-rabbít or donkey anti-goat secondary antibody (Vector, Jackson) was applied for 8 hours (4°C); and the incubation with the ABC reagent was performed overnight (4°C).

For the DAB staining, vibratome sections were first preincubated in DAB (without H_2O_2) for 20 minutes, followed by a 15-minute DAB/H_2O_2 reaction at RT, with Co/Ni enhancement (see above). The sections were then fixed for 7 days in 2% glutaraldehyde in PBS, osmicated, dehydrated, and embedded in araldite (Fluka, Basel, Switzerland). Semithin sections were counterstained with toluidine blue for light microscopy, and ultrathin 100-nm sections were counterstained with uranyl acetate and lead citrate and examined in a Zeiss EM 10 and EM 109 electron microscope.

Quantification of light microscopic immunohistochemistry

A Sony AVT-Horn 3CCD color video camera was used to obtain eight-bit digital images based on a 0–255 (eight-bit) scale of optical luminosity values. Images of both control and axotomized nuclei and for the glass were captured at $\times$10 magnification on a light microscope with 0.06 Neutralfilter. Captured images were run through an algorithm to obtain mean and SD values for optical luminosity. SD was subtracted from the mean for each image (mean-SD algorithm), and the resulting values for axotomized and control sides were each subtracted from the mean optical luminosity values of the glass as described previously (Möller et al., 1996).

Statistical analysis

Statistical analysis for growth cone areas in two group comparisons was performed by using a standard, two-tailed Student's *t*-test or with ANOVA followed by post hoc Tukey in cases of more than two groups.

RESULTS

Facial axotomy causes delayed central axonal sprouting: distribution and orientation

In view of previous reports of neuropeptide-immunoreactive sprout-like structures in the axotomized facial motor nucleus 2 weeks after facial nerve cut (Galiano et al., 2001; Werner et al., 2001; Makwana et al., 2007), our first aim was to provide a detailed mapping of their neuroanatomical distribution. As shown in Figure 1A, facial axotomy after nerve transection at the styloid foramen was associated with the appearance of sprout-like, galanin-immunoreactive (galanin$^+$) neurites inside the brainstem in and around the lesioned facial motor nucleus. A high number of galanin$^+$ sprouts with a 4–10-μm large terminal bulb was observed in the white matter surrounding the lesioned facial motor nucleus, in the ventral corticobasal tract, in the ascending as well as descending part of the intracerebral portion of the facial motor nerve (Fig. 1A,F),

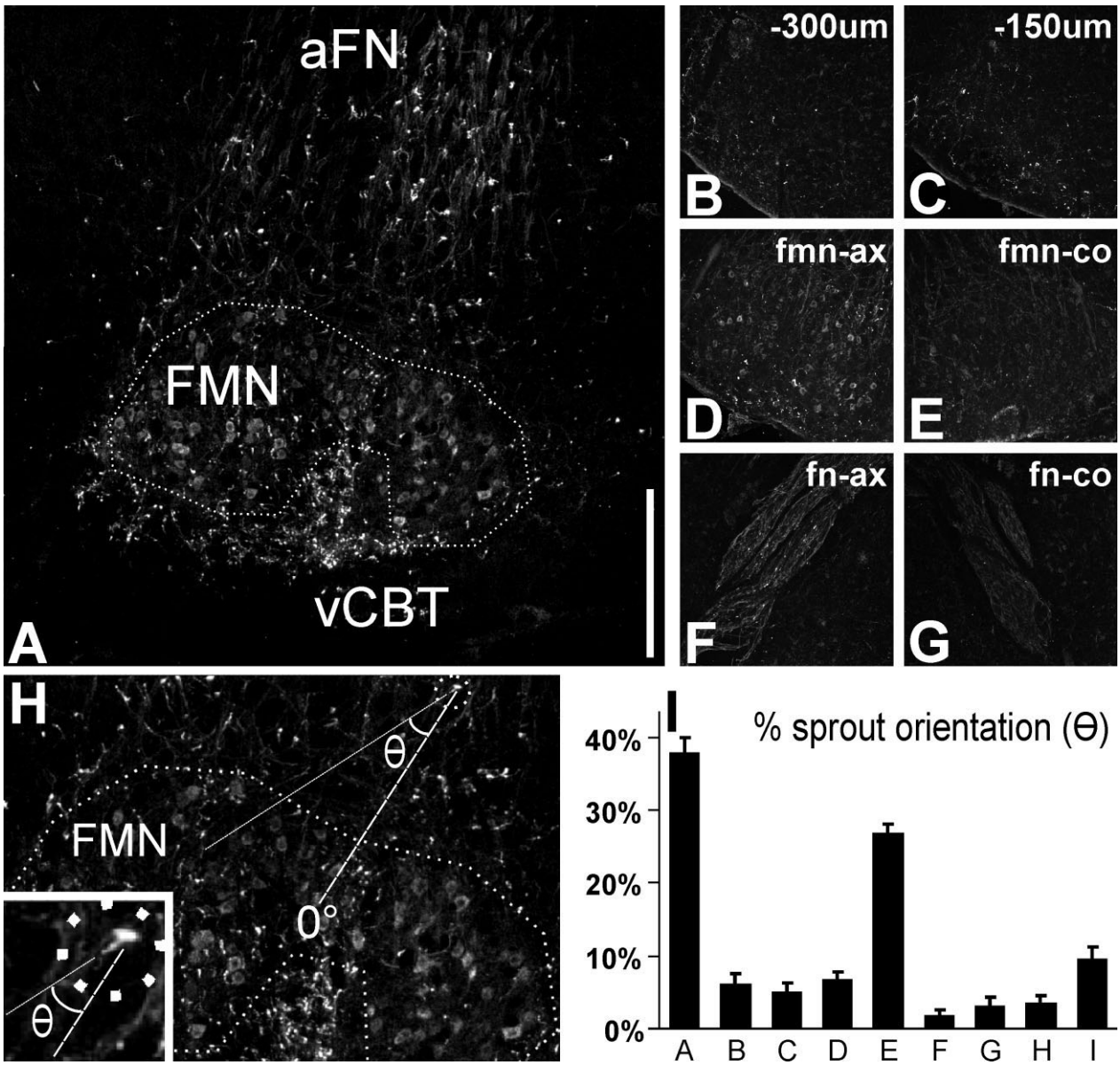

Figure 1. Distribution of galanin-immunoreactive sprouts in and around the facial motor nucleus (FMN), 14 days following facial nerve cut. **A:** Composite of the facial nucleus and surrounding areas; the nucleus outline is indicated by the dotted line. Note the numerous immunoreactive sprouts in the white matter surrounding the lesioned facial motor nucleus, particularly in the ventral corticobasal tract (vCBT) but also in the ascending part of the intracerebral portion of the facial nerve (aFN), and to the medial and lateral of the facial nucleus. **B–G:** Sprout distribution in the rostral direction, from the same ventrolateral brainstem position but 300 μm (B) and 150 μm (C) caudal to the axotomized facial nucleus, the axotomized nucleus (D), and the descending part of the intracerebral facial nerve (F). Note the paucity of strongly stained neurites in the contralateral, uninjured facial nucleus (E) and nerve (G). **H:** The orientation of central sprouts was determined by drawing two lines, one from the center of the terminal bulb to that of the nucleus (dashed line, 0°) and the second from the bulb center to that of the farthest visible part of the stalk and extending it farther into the image (dotted line) and then measuring the angle between the two lines as shown in H. The **inset** in H shows the terminal bulb, the attached stalk, and the orientation of the two lines at higher magnification. **I:** Distribution of the orientation angles for the galanin-immunoreactive sprouts outside the axotomized facial motor nucleus with respect to the nucleus. Percentage of the total number of sprouts, with orientation angles of 0–20°(A), 20–40°(B), 40–60°(C), etc., with 0° pointing directly away from and 180° pointing directly toward the nucleus. Mean ± SEM, n = 4 mice. Note that the most common orientation is the one facing away (A), with the second largest running approximately parallel to the facial nucleus (E). Scale bar = 0.5 mm in A; 0.8 mm for B–G; 0.36 mm for H; 0.1 mm for inset.

and in the medial and lateral parts of the facial nucleus. Some neurites were located as far as 0.5–1.0 mm away from the border of the facial nucleus in the dorsal (Fig. 1A), and 0.3 mm in the caudal (Fig. 1B,C) direction, with the stalk attached to a bulb, usually pointing away from the nucleus (Fig. 1H,I).

Sprouting neurites were also present inside the facial motor nucleus itself, but they were less dense in the horseshoe form of the facial nucleus gray matter, containing the axotomized motoneurons, than in its white matter-like ventral cleavage (Fig. 1H). A similar distribution was also observed for the CGRP$^+$ sprouts, but their density was considerably lower compared with that of the galanin$^+$ fibers. Although individual galanin$^+$ and CGRP$^+$ neurites were observed in the contralateral facial nucleus (Figs. 1E, 2H), these neurites lacked the typical appearance of sprouts with the engorged terminal bulb. These sprouts were also absent in the intracerebral part of the contralateral nerve (Fig. 1G); the ipsi-and contralateral pyramidal tract (Fig. 2H); the dense neurite network in the dorsal part of the spinal nucleus of the trigeminal nerve (Fig. 2G); or in other brainstem, cerebellar, or cortical white matterstructures (not shown). CGRP and galanin immunoreactivities were also present in adjacent axotomized motoneurons, each labeling approximately 40–45% of the total facial motoneuron pool (Moore, 1989; Raivich et al., 1995), but the intensity of the cell body labeling was weaker than that observed in the sprouts.

To explore the overall orientation of these central sprouts, we next examined the orientation angle of galanin$^+$ sprouts outside the facial nucleus on brainstem sections containing the axotomized nucleus. The orientation was determined as the angle between the line from the facial nucleus center to the center of the axonal bulb and a second line from the bulb center to the farthest visible part of the attached axonal stalk, as shown in Figure 2H and H, inset. The angles were determined at $\times$10 magnification, using confocal images from brainstems of four control C57Bl/6 mice, 14 days after facial nerve cut, and for each animal subgrouped into one of the nine categories A–I, from 0 ° to 20 ° (pointing outward, A), to 160–180° (pointing to the center of the facial nucleus, I). Angles greater than 180° (second line to the left of the central line, instead of to the right), were entered by subtracting 180°, i.e., 265° was entered as 95°. As shown in Figure 1, sprout angle distribution was very nonuniform, with the frequency in three groups (A, E, and I) rising above that in the directly adjacent groups. In total, these three groups were responsible for approximately 70% of the sprouts. The A group with sprouts facing away from the nucleus was the largest (39% $\pm$ 3%, mean $\pm$ SEM), followed by groups E, which contained sprouts oriented approximately parallel to the nucleus (24% $\pm$ 1%), and I, with the sprouts directly or almost directly facing toward the nucleus (8.5% $\pm$ 2.2%). The number of sprouts in the adjacent and intermediate categories was underrepresented. Although the number of sprouts in B was slightly higher (8.7% $\pm$ 0.6%) than in I, these two groups were not adjacent. In comparisons with the directly adjacent groups (A vs. B, E vs. D or F, and I vs. G) the frequency in A, E, and I was each time both significantly and very clearly higher ($P < 5\%$, one-way ANOVA followed by post hoc Tukey test). Although the numbers were considerably lower, the frequencies in the two segments directly adjacent to each of the three peaks, A, E and I, again showed similar proportions of approximately 3:2:1 for the outward pointing (B,C, 15.2%), to roughly perpendicular (D,F, 8.3%), to inward pointing (G,H, 4.5%) groups.

Motoneuron origin of central axonal sprouts

To determine whether the bulb-carrying neurites originated from the lesioned motoneurons, axotomized neurons were retrogradely labeled with a 1% solution of the dual, anterograde and retrograde, tracer Mini-Ruby (Fig. 2A). As shown in the composite of the ventral brainstem in Figure 2H, application of the tracer on the proximal nerve stump surface immediately after facial nerve cut led to a highly selective labeling of neuronal cell bodies and their proximal branches in the ipsilateral facial motor nucleus.

Double labeling with galanin immunoreactivity demonstrated clear Mini-Ruby fluorescence inside a fraction of galanin$^+$ sprouts around the axotomized facial motor nucleus (Fig. 2B,H, insets). Similar double labeling was also present inside the intracerebral part of the ipsilateral facial nerve (Fig. 2F, insets). Finally, this colocalization was also observed with the CGRP$^+$ sprouts (Fig. 2C). Compared with the neuropeptide immunoreactivity, Mini-Ruby fluorescence was more concentrated to the central parts of the axonal bulb, with weaker and more fragmented labeling of the neighboring axonal stalk.

Quantification of the double-labeled sprouts directly outside the facial motor nucleus, shown in Table 2, demonstrated clear Mini-Ruby fluorescence in 19% $\pm$ 3% of the galanin$^+$ and 42% $\pm$ 9% of the CGRP$^+$ sprouts and, in addition, 39% + 1% of the VAChT$^+$ sprouts in adjacent, galanin-, CGRP-, and VAChT antibody-stained brainstem sections ($P < 5\%$ ANOVA followed by Tukey post hoc test, for differences vs. the galanin$^+$ sprouts; n = 4 C57Bl/6 mice, three sections per animal). In the reverse experiment, quantification of the neuropeptide immunoreactivity showed that 64% $\pm$ 3% of the identified, Mini-Ruby fluorescent sprouts also exhibited galanin, 44% $\pm$ 10% CGRP, and 44% $\pm$ 2% VAChT immunoreactivity (not significant). This double labeling, Mini-Ruby/CGRP, Mini-Ruby/VAChT, or Mini-Ruby/galanin, was not observed outside the main areas of central axonal sprouts. Thus the ipsilateral spinal nuclei of the trigeminal nerve (Fig. 2G), contralateral facial nerve (Fig. 2F), or contralateral facial nucleus (Fig. 2H, right side) were all devoid of axonal Mini-Ruby fluorescence.

However, in addition to sprouts, Min-Ruby fluorescence was also occasionally present in large and ellipsoid

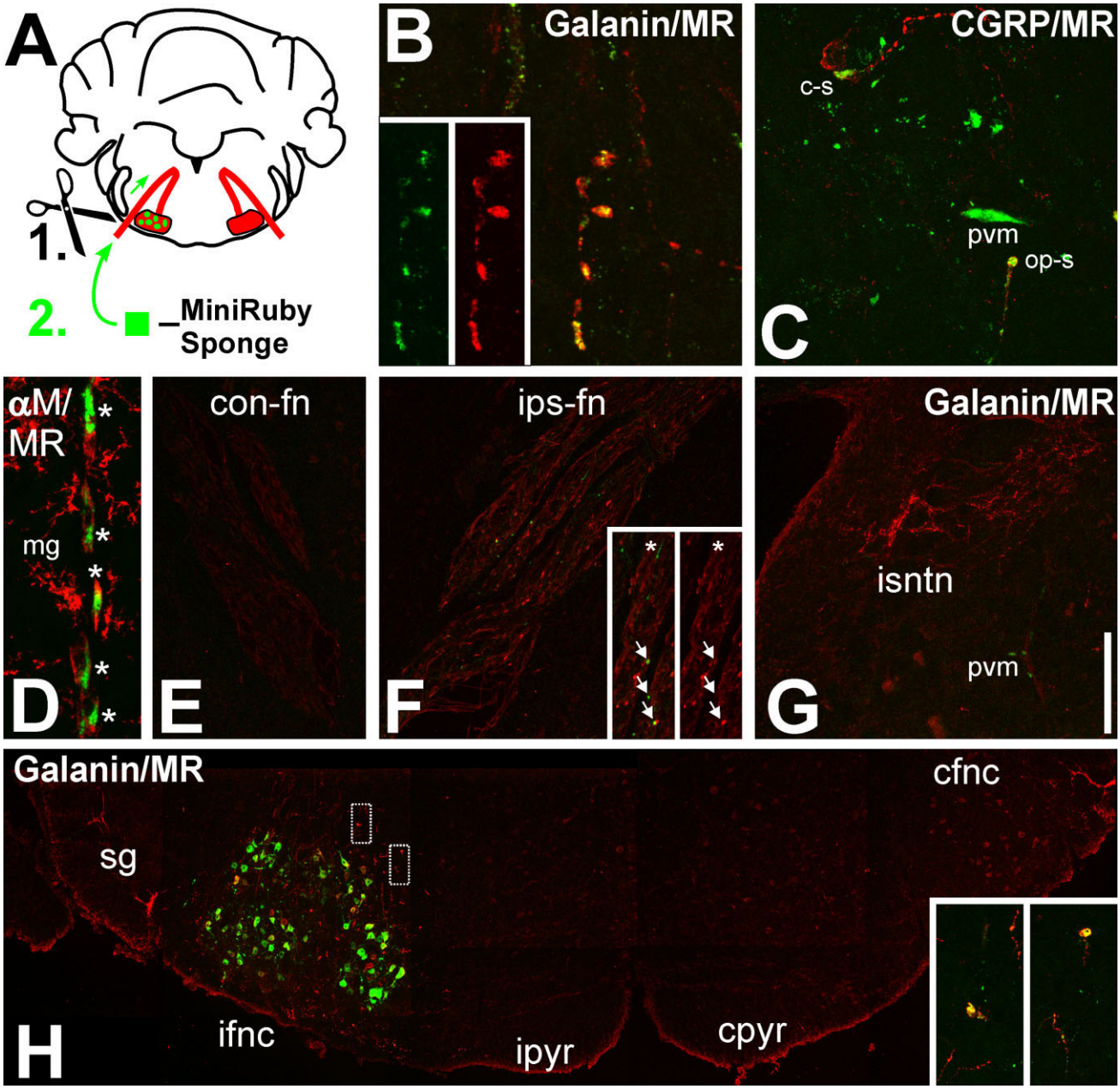

Figure 2. Demonstration of central axonal sprout origin using Mini-Ruby, a dual anterograde/retrograde tracer. **A:** Schematic summary. A gelfoam sponge soaked in 1% Mini-Ruby solution was applied onto the fresh, proximal cut end of the facial nerve, followed by retrograde transport to axotomized motoneurons and a 14-day survival. **B,C:** High magnification of Mini-Ruby (green) colocalization with the immunoreactivity (IR) for the neuropeptides galanin (B) and CGRP (C) (red) in axonal sprouts just outside the axotomized facial motor nucleus. The double-labeled sprout in B and the bottom sprout in C are outward pointing (op-s); the top sprout in C is oriented in parallel to the center of the nucleus ("cruising," c-s). The **insets** in B show the individual red and green fluorescence channels. In C, Mini-Ruby is also incorporated by perivascular macrophages (pvm). **D:** Mini-Ruby uptake in a string of alphaMbeta2 integrin (aM)-positive (red) perivascular macrophages (*) lining a cerebral blood vessel. The neighboring aM-positive and ramified microglia (mg) are devoid of Mini-Ruby. **E–G:** Double fluorescence for Mini-Ruby and galanin-IR in the descending intracerebral part of the contralateral facial nerve (E); the axotomized, ipsilateral facial nerve (F); and the ipsilateral spinal nucleus of trigeminal nerve (G, isntn). The **insets** in F show a higher magnification of the facial nerve (left, red and green; right, red only fluorescence). Note the double-labeled sprouts in the axotomized nerve (arrows) and their absence in the neighboring trigeminal nerve nucleus and contralateral nerve. The asterisk points to a Mini-Ruby^{+} but galanin^{-} sprout. As in C, Mini-Ruby is frequently present in the populations of perivascular macrophages associated with larger blood vessels (D, pvm). The micrographs in E and F show the same galanin labeling motif as in Figure 1E,F but combine it with the Mini-Ruby fluorescence. **H:** Composite of Mini-Ruby and galanin-IR fluorescence in the ventral brainstem across the ipsilateral substantia gelatinosa, the ipsilateral and contralateral facial motor nuclei (ifnc, left; cfnc, right, respectively), and the ipsilateral and contralateral pyramidal tracts (ipyr and cpyr). Mini-Ruby neuronal cell body labeling is strictly limited to the axotomized facial motor nucleus, with a high density of galanin-positive sprouts in the surrounding tissue. Note the absence of both in the pyramidal tracts and the contralateral facial nucleus. The **insets** show higher magnifications for galanin/Mini-Ruby double labeling (yellow) of two sprouts just dorsal of the axotomized facial nucleus; their positions in the composite are indicated by the rectangles in H. A magenta/green version of Figure 2 is available as Supporting Information Figure 1. Scale bar = 10 μm in B, 45 μm in C and D, 270 μm in E–G; 350 μm in F insets.

TABLE 2.
Colocalization of Mini-Ruby (MR) With Galanin and CGRP-Positive Growth Cones (n = 4 Animals, Three Facial Nucleus Sections per Animal; Mean ± SEM)

Growth cone neurochemical marker (NCM)	MR^+NCM^+/NCM^+ (%)	MR^+NCM^+/MR^+ (%)
Galanin	19 ± 3	64 ± 3
CGRP	42 ± 9[1]	44 ± 10
VAChT	39 ± 1[1]	44 ± 2

[1] $P < 5\%$, one-way ANOVA, followed by Tukey post hoc test for differences in the frequency to $MR^+/galanin^+$ growth cones. The percentages are derived from, on average, approximately 50-60 double-labelled growth cones per animal and axotomized facial motor nucleus.

perivascular macrophages (Fig. 2C,G). As shown in Figure 2D, this Mini-Ruby labeling colocalized with the alphaM-beta2 immunoreactivity in the perivascular macrophages and was easy to differentiate from the smaller Mini-Ruby-fluorescent axonal bulbs inside the neural parenchyma. The alphaMbeta2$^+$ parenchymal microglia were uniformly Mini-Ruby$^-$.

Time course after injury and effects of reinnervation and recut

Comparison of the galanin-and CGRP-immunostained, axotomized facial motor nuclei 1–42 days after facial nerve cut with unoperated controls (day 0) revealed a transient sprouting pattern, shown in Figure 3A–AF. No sprouts were observed in the unoperated facial nuclei or 1–4 days after nerve cut. A moderate number of galanin$^+$ and CGRP$^+$ sprouting neurites was observed at day 7; these became much more common at day 14, decreased in number at day 21, and disappeared by 42 days after nerve injury and the ensuing regeneration (Fig. 3A–F,AG,AI).

As shown in Figure 3AH, automatic quantification of the intensely neuropeptide-immunofluorescent end-bulbs in and around the facial motor nucleus using confocal scanning and the GCD algorithm (see Materials and Methods) reproduced this time course for galanin, with a peak density at day 14, with 5,200 parts per million (ppm) or 0.52% of the total area of the 1 mm × 1 mm region with the facial nucleus at its center covered with galanin$^+$ end-bulb structures. However, the GCD algortihm was associated with a low-level "noise" of 200–600 ppm on the contralateral side throughout the time course, or approximately 4–12% of the peak signal levels at day 14.

Direct visual counting of the CGRP$^+$ growth cones (Fig. 3AI) showed a time course with a shape similar to that with galanin (Fig. 3AG). Maximal levels were observed at day 14, with 24 ± 5 CGRP$^+$ sprouts per 20-μm section, approximately 3–4-fold less than with galanin in the directly adjacent sections (89 ± 8). Unlike the case with galanin, quantification of the CGRP$^+$ end-bulbs with the GCD algorithm revealed a comparatively broader and statistically significant elevation of detected structures on days 4–21 compared with the contralateral side (Fig. 3AJI). However, the overall levels (200–260 ppm) were much lower, and the more granular (Nissl-shoal) appearance of the CGRP immunoreactivity in neuronal cell bodies could have made automatic growth cone detection more complicated. For this reason, both quantitation methods, visual counting and GCD algorithm, were used side by side in the following experiments.

Because the time course of sprouting, with a peak at day 14, occurred at roughly the same time as the morphological reinnervation and functional recovery in the facial axotomy model (Gilad et al., 1996; Werner et al., 2000; Raivich et al., 2004), we next sought to determine whether the appearance of sprouts is due to target reinnervation. Reinnervation is known to occur earlier, more promptly, and with less error after crush than after cut (Nguyen et al., 2002; Witzel et al., 2005), so we first examined the differential effects of the facial nerve crush vs. cut on galanin$^+$ growth cone profiles at days 7, 10, and 14. Here, facial nerve crush induced the appearance of galanin$^+$ spouts that peaked at day 10, with 800 ppm of the total area (Fig. 4A). Compared with crush, nerve transection produced a more robust sprouting response, with a slight but not significant increase at days 7 and 10 and an almost 10-fold increase at day 14 ($P < 5\%$, Student's *t*-test). As shown in Figure 4A,C, automatic quantification with the GCD algorithm (Fig. 4A) and visual counting (Fig. 4C) revealed very similar changes in the timing of sprouting changes and

Figure 3. **A–AJ:** Time course of the appearance (A–AF) and quantification (AG–AJ) of galanin- and CGRP-immunoreactive sprouts in the facial motor nucleus, 1–42 days after facial nerve axotomy; day 0 are uninjured controls. A–AF show the immunofluorescence in injured facial nucleus at low magnification (A,E,I,M,Q,U,Y,AC for galanin, and C,G,K,O,S,W,AA,AE for CGRP) and at ×4 or ×8 higher magnification for galanin (B,F,J,N,R,V,Z,AD) and CGRP (D,H,L,P,T,X,AB,AF). Note the massive increase in the neuropeptide-labeled sprouts (arrows) at days 7–21; arrowheads point to neighboring motoneuron cell bodies. AG–AJ: The graphs at right show the total number of galanin-and CGRP-immunoreactive sprouts per section (AG and AI, respectively) and the quantification of the area taken by the galanin-and CGRP-immunoreactive sprouts (AH, AJ) in parts per million (ppm). Mean ± SEM, n = 3 animals per group in AG and AI, n = 4 in AH and AJ). *$P < 0.05$, Student's *t*-test compared with the unoperated, contralateral side. In the case of galanin, both parameters, number (AG) and area (AH), show a sharp peak at day 14. The same also holds true for the CGRP$^+$ sprout number (AI), but the CGRP$^+$ area recognized by the Optimas GCD algorithm (AJ) shows a broader, elevated plateau between day 4 and day 21. Scale bar = 250 μm in first and third columns; 0.063 μm in the second column; 0.032 μm in fourth column.

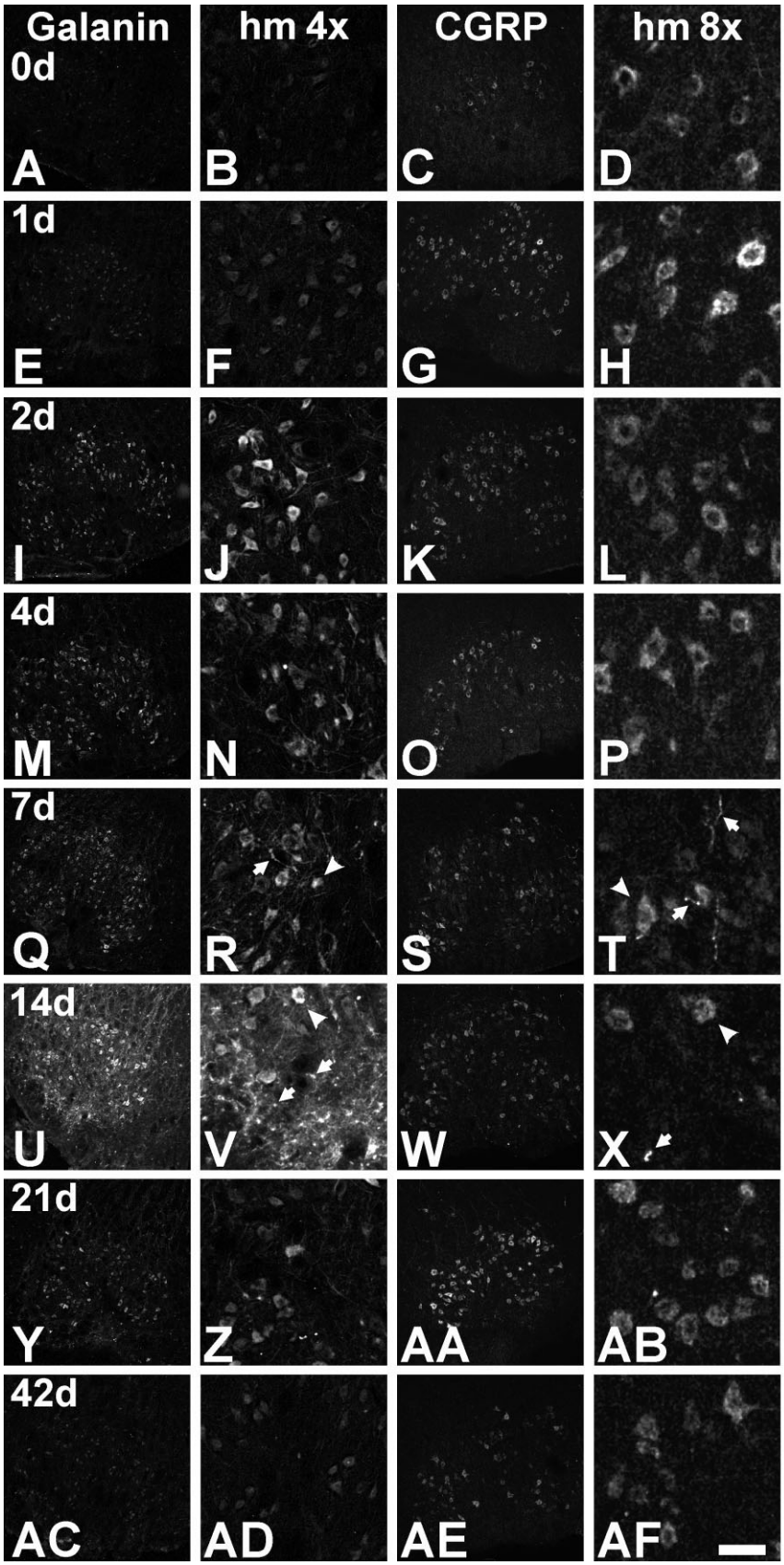
Galanin
hm 4x
CGRP
hm 8x
0d
A
B
C
D
1d
E
F
G
H
2d
I
J
K
L
4d
M
N
O
P
7d
Q
R
S
T
14d
U
V
W
X
21d
Y
Z
AA
AB
42d
AC
AD
AE
AF

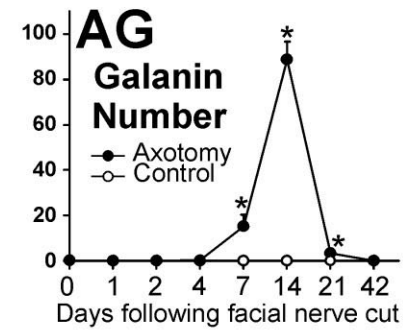
AG
Galanin
Number
Axotomy
Control
100
80
60
40
20
0
0 1 2 4 7 14 21 42
Days following facial nerve cut

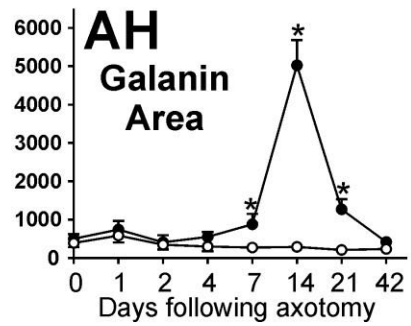
AH
Galanin
Area
6000
5000
4000
3000
2000
1000
0
0 1 2 4 7 14 21 42
Days following axotomy

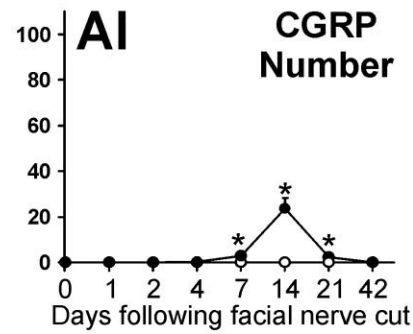
AI
CGRP
Number
100
80
60
40
20
0
0 1 2 4 7 14 21 42
Days following facial nerve cut

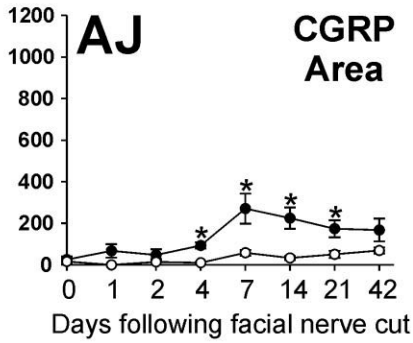
AJ
CGRP
Area
1200
1000
800
600
400
200
0
0 1 2 4 7 14 21 42
Days following facial nerve cut

Figure 3

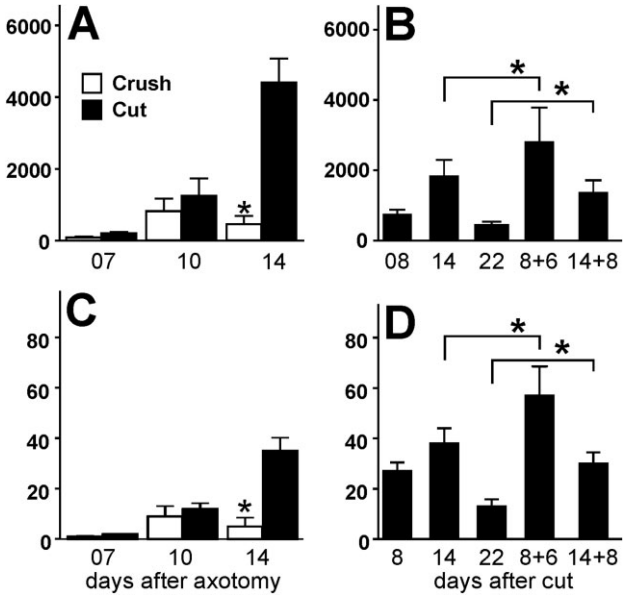

Figure 4. A–D: Central axonal sprouting depends on the mode of injury. A,C: After facial nerve crush, the sprout area in ppm (A) and the number of sprouts per section (C) reach a moderate peak at day 10 and after cut a much higher peak at day 14. *$P < 0.05$, Student's *t*-test for crush vs. cut (n = 3 animals per group, mean ± SEM). B,D: Additional injury exacerbates central axonal sprouting following facial nerve cut—both in total area (B) and in the number of sprouts (D)—compared with the same total cut period (8 + 6 vs. 14 days, 14 + 8 vs. 22 days). *$P < 0.05$, one-way ANOVA and post-hoc Tukey, n = 4–5 animals per group.

differences in the response to crush vs. cut response, confirming the cross-validity of both techniques for the galanin$^+$ sprouts.

To determine further whether the appearance of growth cones was due to the onset in reinnervation of peripheral targets occurring 8–14 days after injury, we next examined the effects of single facial nerve cut vs. a second transection. The facial nerve was recut 1 mm below the initial lesion (n = 5 animals per group) on day 8 with survival to day 14 or was recut on day 14 with survival to day 22 and compared with normal animals 8, 14, and 22 days after facial nerve cut, which served as controls (Fig. 4B,D). Surprisingly, the growth cones were not abrogated; in fact, the area under growth cone profiles was 1.5–2-fold greater than in control day 14 or day 22 postcut brainstems ($P <$ 2%, ANOVA). As in Figure 4A,C, very similar quantitative effects were observed with the GCD algorithm (Fig. 4B) and visual counting (Fig. 4D).

Preliminary studies with shorter recut times (1, 2, and 4 days) and total transection time of 14 days revealed that the growth cone profiles were more numerous than after a simple day 14 cut, but the effects were less pronounced than in 8 + 6 vs. 14, or 14 + 8 vs. 22 (data not shown). Finally, retrograde tracing experiments with application of MiniRuby to the ipsilateral whiskerpad, the principal peripheral target of the facial nerve maxillary and zygomatic branches on day 12, showed some motoneuron cell body labeling but failed to be incorporated into the facial growth cones at day 14 (data not shown), unlike the Mini-Ruby labeling applied on the freshly cut facial nerve stump, shown in Figure 2B,C,E and the inset in Figure 2H.

Molecular markers and ultrastructure

To define the molecular markers of axotomy-induced sprouts, we next examined the presence of VAChT, microtubule-associated protein 2 (MAP2), synaptophysin, and NFH as cholinergic, dendrite, presynaptic, and panneurite markers, respectively (Fig. 5, three left columns) as well as the CD44 hyaluronic acid receptor and the alpha4, alpha5, alpha6, alpha 7, and beta1 subunits of the beta1 integrin family (Fig. 5, three right columns), using double immunofluorescence with galanin, CGRP, or VAChT (Fig. 5G–I,S–Y). Markers labeled with rabbit polyclonal antibodies (MAP2, NFH, alpha7) were double stained with guinea pig antibodies against VAChT, and those labeled with rat monoclonal antibodies (alpha4–6, beta1, CD44) were double stained with galanin or CGRP.

The CGRP$^+$ (Fig. 5A–C) and galanin$^+$ (Fig. 5D–F) sprouts colocalized with VAChT immunoreactivity, confirming their cholinergic phenotype. They were also positive for CD44 (Fig. 5V–Y) and beta1 (Fig. 5S–U) but not for alpha4, alpha5 or alpha6 (not shown). Most VAChT sprouts were also positive for synaptophysin (Fig. 5P–R), and many were alpha7$^+$, even though some large and distended alpha7$^+$ sprout end-bulbs were VAChT$^-$ (Fig. 5G–I). VAChT$^+$ sprouts did not colocalize with NFH (Fig. 5G–I) or MAP2 (Fig. 5M–O) immunoreactivity, suggesting that most sprouts are derived from cholinergic neurons, that they do not colocalize with typical components of dendritic (McDermid et al., 2004) or axonal shaft cytoskeleton, and that they express regeneration-associated CD44 and alpha7beta1 integrin cell adhesion molecules (Werner et al., 2000; Raivich et al., 2004). Similarly pronounced, regeneration-associated immunoreactivity was also observed on the Mini-Ruby-labeled axonal sprouts, shown in Figure 5Z–AB for the alpha7, in Figure 5AC–AE for beta1, in Figure 5AF–AH for CD44, and in Figure 5AI–AK for VAChT, reconfirming the facial motoneuron origin of these neurochemically tagged structures.

Many alpha7$^+$, galanin$^+$, and VAChT$^+$ sprout end-bulbs were particularly pronounced in the basal white matter located ventrally of the axotomized facial motor nuclei, so we next explored their utrastructural morphology by transmission electron microscopy (EM), 14 days after facial nerve cut (Fig. 6A,B). Starting with alpha7, immunolabeling against the intracellular part of the alpha7 integrin subunit revealed strong cytoplasmic staining surrounding numer-

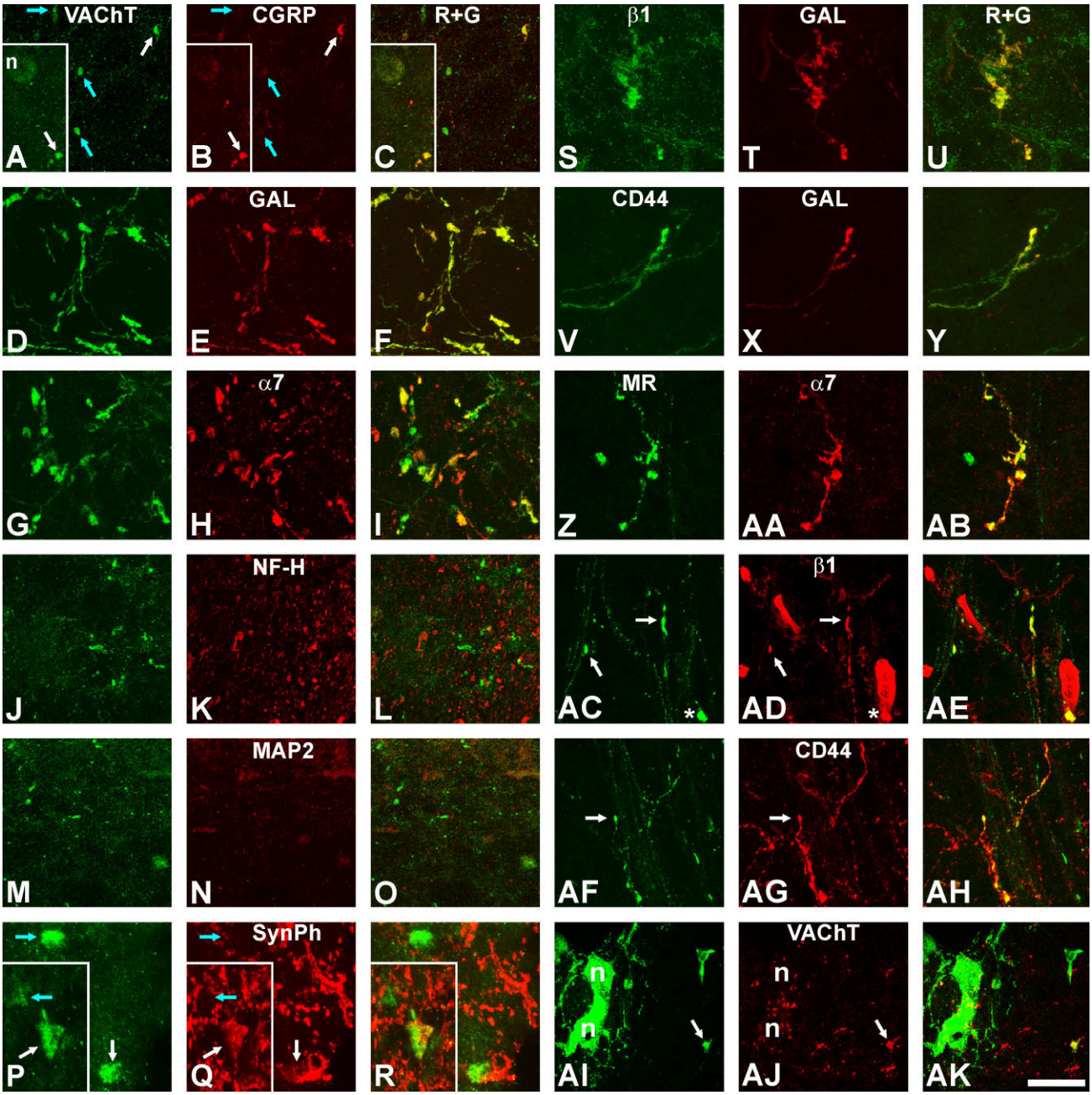

Figure 5. Molecular characterization of growth cones in the facial nucleus 14 days following facial nerve cut. **A–R:** Immunoreactivity for vesicular acetylcholine transporter (VAChT), double labeling with CGRP (A–C), galanin (D–F), alpha7 integrin subunit (G–I), neurofilament heavy (NFH) isoform (J–L), microtubule-associated protein-2/MAP2 (M–O), and synaptophysin/SynPh (P–R) immunoreactivities. VAChT$^+$ sprouts were very frequently positive for galanin, frequently also for alpha 7 and synaptophysin, and more rarely for CGRP immunoreactivity (white arrows in A–C, blue arrows mark single-labeled VAChT$^+$ sprouts). Note the absence of double labeling for NFH and MAP2. A–C and P–R are inside the facial motor nucleus, D–L in the adjacent ventral white matter, and M–O at the gray/white matter interface. A–C and P–R are composite micrographs, to illustrate the colocalization of some but not all VAChT$^+$ sprouts with CGRP and synaptophysin. **S–Y:** Colocalization of galanin-positive sprouts with the beta1 integrin subunit (S–U) and with CD44 (V–Y). **Z–AK:** Colocalization of Mini-Ruby-labeled growth cones with the alpha7 (Z–AB) and beta 1 (AC–AE) integrin subunits, CD44 (AF–AH), and VAChT (AI–AK). White arrows point to double-labeled sprouts in AC,AD, in AF,AG, and in AI,AJ). Asterisks in AC and AD label a Mini-Ruby$^+$, perivascular macrophage. Micrographs in AI–AK are from the border region between facial nucleus (left) and medial white matter and also show two adjacent, Mini-Ruby-labeled motoneurons (n) at left, surrounded by large, VAChT$^+$ synapses. Z–AH are inside the dorsal white matter, next to the facial nucleus. A magenta/green version of Figure 5 is available as Supporting Information Figure 2. Scale bar = 50 μm for A–C,J–L; 27 μm for Z–AB,AI–AK; 12.5 μm for P–R; 40 μm in all other micrographs.

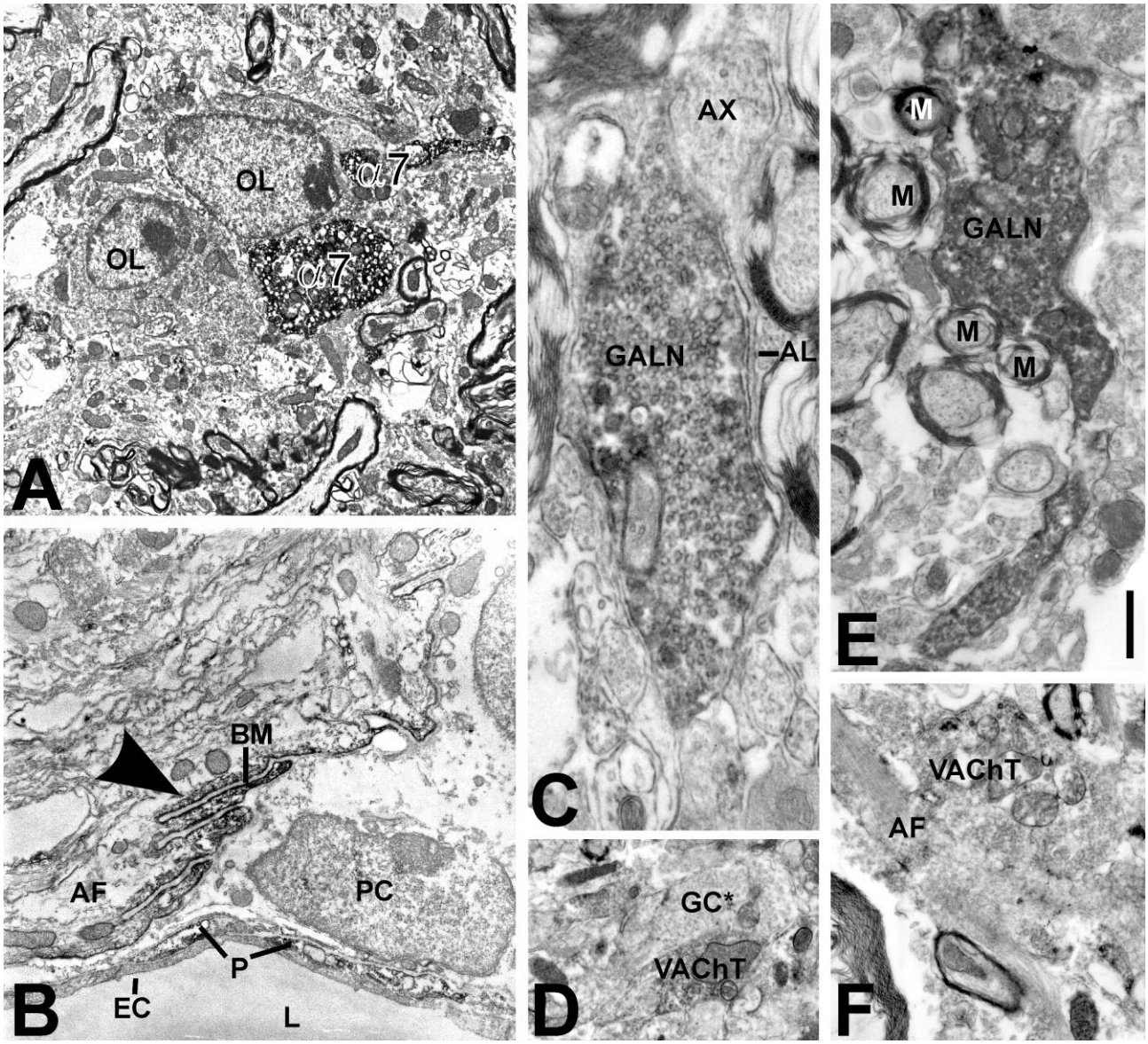

Figure 6. Ultrastructure of axonal growth cones and their cellular contacts using alpha7 (A,B), galanin (C,E), and VAChT (D,F) immunoreactivity in the white matter surrounding the facial motor nucleus, 14 days following facial nerve cut in WT animals. **A:** Intensely cytoplasmically stained axonal growth cones (alpha7), containing numerous (unstained) mitochondria and synaptic vesicles and contacting adjacent oligodendrocytes (OL). **B:** Strong alpha7 immunoreactivity in submembranous astrocyte cytoplasm (arrowhead) next to the finger-like protrusions of the basal membrane (BM). Some alpha7 immunoreactivity was also present in blood vessel pericytes (P). L, blood vessel lumen; EC, endothelial cell; PC, perivascular cell; AF, astrocyte fibrils. **C,E:** Galanin (GALN)-immunoreactive growth cones, here contacting astrocyte lamella (AL; C), unmyelinated axons (AX; C), and numerous myelinated axons (E). **D,F:** VAChT-immunoreactive axonal sprouts growing alongside a VAChT-negative (GC*) growth cone (D) and an astrocyte fibril (AF)-containing process (F). Scale bar = 1 μm for A,B,F; 0.35 μm for C; 1.2 μm for D; 0.6 μm in E.

ous mitochondria and vesicles, demarcating the 2–5-μm large structures characteristic of growth cone morphology and the associated 0.3–0.5-μm thin axonal stalks that were frequently directly in contact with neighboring alpha7-negative oligodendroglial surfaces (Fig. 6A). There was no alpha7 immunoreactivity on the associated myelin or myelinated axons (Fig. 6A), blood vessel endothelia, or large perivascular cells (Fig. 6B). However, some submembraneous alpha7 immunoreactivity was also present on the small pericytes and the astrocytic processes contacting the perivascular basal membranes (Fig. 6B).

Similar sprout ultrastructure was also observed using immunoreactivity for galanin (Fig. 6C, E) and VAChT (Fig. 6D, F). To determine the approximate frequency of different contacts, we analyzed 39 galanin^{+} and 57 VAChT^{+} sprouts at ×10,000 magnification (Table 3). Assessment with these latter, common and unambiguously neuron-specific markers revealed frequent growth cone contacts

TABLE 3.
Utrastructural Growth Cone Contacts

Detected growth cone immunoreactivity	Galanin positive (%)	VAChT positive (%)
Contact with myelin	56 (22/39)	54 (31/57)
Oligodendroglial cell body	3 (1/39)	0 (0/57)
Astrocyte lamella	95 (37/39)	91 (52/57)
Filamentous astrocyte process	23 (9/39)	21 (12/57)
Neighboring axon	97 (38/39)	100 (57/57)
Another growth cone	15 (6/39)	39 (22/57)[1]

[1] $P < 2\%$, χ^2 test comparing this contact type for galanin$^+$ vs. VAChT$^+$ growth cones. Galanin$^+$ and VAChT$^+$ can contact several different structures at the same time, so the total number of different contacts can be higher (approximately three times higher) than the number of the labelled growth cones in either column.

with neighboring unmyelinated axons and astrocyte lamellae (Fig. 6C), other growth cones (Fig. 6D), myelin sheaths (Fig. 6E), and large astrocyte processes containing astrocyte fibrils (Fig. 6F). As shown in Table 3, quantification of identified growth cones and their contacts in the electron microscopic sections of perifacial ventral white matter revealed that they were particularly frequent with neighboring unmyelinated axons (97–100%), astrocyte lamella (91–95%), and outer myelin sheaths (54–56%), and with lower frequency with other growth cones, fibrillar astrocyte processes (21–23%), and oligodendroglial cell bodies (0–3%). This frequency of cellular contacts was very similar for the galanin$^+$ and VAChT$^+$ sprouts. The only exception were contacts with other growth cones, which were approximately 2.5-fold more common in the VAChT$^+$ sprouts (39%) than in galanin$^+$sprouts, with 15% ($P < 2\%$, χ^2 test).

Effects of lipopolysaccharide-induced inflammation and alpha7, brain c-Jun, and TNFR1/2 deletions

Previous studies with the facial axotomy model examining neuronal cell death (Möller et al., 1996; Raivich et al., 2002), leukocyte influx (Raivich et al., 1998; Bohatschek et al., 2001), bystander-activation inflammatory changes in neighboring microglia, and induction of late neuronal regeneration-associated molecules such as galanin and beta1 integrin subunit (Kloss et al., 1999) showed that these events also peak at day 14, coinciding with the currently detected maximum in intracerebral facial axonal sprouting. To determine their effects on the delayed facial sprouting, we next examined the changes resulting from specific gene deletion mutants for alpha7, brain c-Jun, and TNF receptor types 1 and 2 (TNFR1/2) gene deletions, and LPS-induced inflammation, which were previously shown to affect cell death, regeneration, bystander activation, and neural leukocyte recruitment.

In the case of c-Jun, preliminary data suggested a reduction of sprouting in the absence of brain c-Jun (Raivich et al., 2004; Supp. Info. Fig. 2). In the current study, direct quantification of growth cone area using GCD algorithm and visual counting confirmed this effect (Fig. 7A–C), revealing a 97% decrease in area and a 96% decrease in the number of galanin$^+$ sprouts in mice lacking brain c-Jun ($P < 1\%$, Student's *t*-test). Deletion of the alpha7 integrin subunit (Fig. 7G–I) caused a 45% increase in area and 50% increase in the number of galanin$^+$ sprouts in the –/–mice ($P < 5\%$); that of TNFR1/2 (Fig. 7J–L) was associated with a 39% increase in area but minimal change (–3%) in the number of sprouts, with neither change reaching the level of statistical significance ($P = 10.5\%$ and 92%, respectively). Systemic application of 1 mg *E. coli* lipopolysaccharide (LPS) in 0.9% saline (Fig. 7M–R) with a 0.5-, 1-, or 2-day interval preceding day 14 caused an approximately 50% reduction in the area of galanin$^+$ sprouts ($P < 2\%$, one-way ANOVA followed by post hoc Tukey); the effect disappeared at the 4-day interval. Injection of saline alone with a 1-day interval did not affect sprouting (Fig. 7O). Direct visual counting revealed similar, approximately 40% decrease in the number of sprouts 0.5–2 days following exposure to LPS ($P < 5\%$, one-way ANOVA, post hoc Tukey).

Because absence of brain c-Jun also strongly diminished the postaxotomy increase in neuronal galanin immunoreactivity in a previous study (Raivich et al., 2004), it is possible that the currently detected effect of c-Jun was due to galanin-presumptive sprouts carrying very little galanin immunoreactivity and thus escaping detection. This problem appears to be specific for galanin and c-Jun; deletion of alpha7 did not appear affect the overall galanin immunoreactivity (Werner et al., 2000). In the current study, we reconfirmed this lack of effect on the overall galanin immunofluorescence (IF) in the axotomized facial motor nucleus in the alpha7 mutants [10.0 ± 0.4 vs. 9.6 ± 0.7 in optical luminosity values (OLV) for the IF in alpha7+/+ and –/–mice, respectively; $P = 61\%$] and noted similar lack of effect in TNFR1/2 mutants (8.4 ± 0.8 vs 8.6 ± 0.5, $P = 86\%$), or the application of LPS (8.76 ± 0.61 for control, 9.51 ± 0.80 for 0.5 days, 9.88 ± 1.11 for 1 day, 9.55 ± 0.61 for 2 days, and 9.53 ± 0.89 for 4 days, respectively; $P = 90\%$ in one-way ANOVA). In general, brightly fluorescent axonal growth cones showed an approximately 3–3.5-fold higher staining compared with the whole facial motor nucleus (0.50–0.55 in $\log_{10}$ relative intensity of staining and contrast/RISC units). However, unlike the results in the interleukin-6 deletion study (Galiano et al., 2001), we did not observe a statistically significant change in the RISC values of the mutants (jun, alpha7, TNFR1/2) compared with their wild-type littermates (*t*-test) or in LPS-injected animals compared with controls (one-way ANOVA).

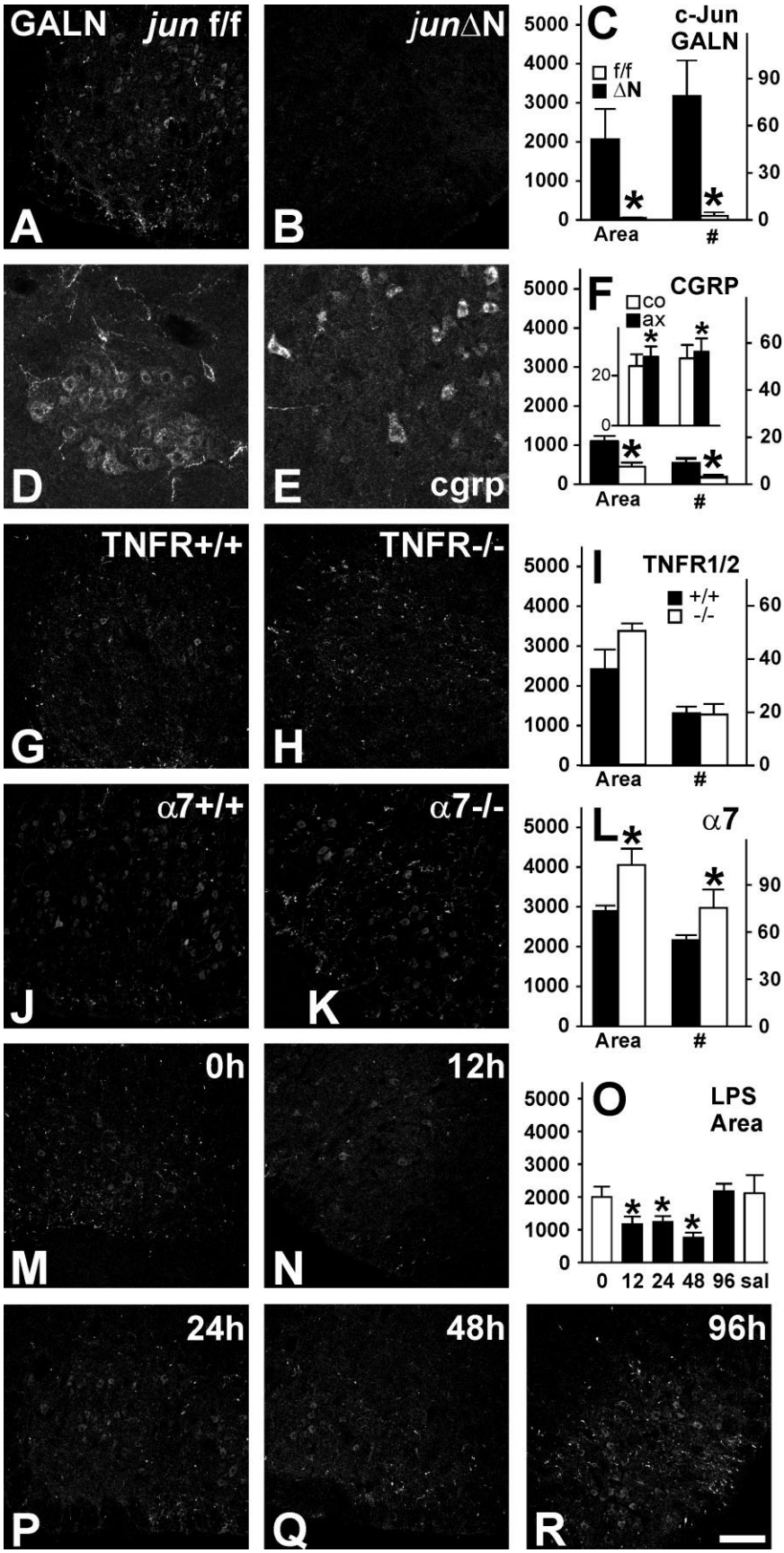
GALN jun f/f
A
junΔN
B
C
c-Jun
GALN
f/f
ΔN
5000
4000
3000
2000
1000
0
90
60
30
0
Area
#
D
E
cgrp
F
CGRP
co
ax
20
0
60
40
20
TNFR+/+
G
TNFR-/-
H
I
TNFR1/2
+/+
-/-
α7+/+
J
α7-/-
K
L
α7
0h
M
12h
N
O
LPS
Area
0 12 24 48 96 sal
24h
P
48h
Q
96h
R

Figure 7

In line with previous data (Moore, 1989; Raivich et al., 1995), quantitative experiments on total CGRP immunoreactivity did reveal constitutively strong staining on the control side and, at 14 days after axotomy, a moderate though significant increase on the injured side in the control *jun*$^{f/f}$ (Fig. 7F, inset, two left bars) as well as in the brain Jun-deficient mice (Fig. 7F, inset, two right bars; $P < 1\%$, Student's *t*-test). Moreover, neither the control nor the axotomized side nor the increase in CGRP staining on the axotomized side was affected by deletion of brain c-Jun.

To validate the effect of brain c-Jun on facial axonal sprouting, we therefore examined the effects on the CGRP^{+} sprouts. As shown in Figure 7D,E, deletion of brain c-Jun brought on a visible reduction in sprouts labeled with CGRP immunoreactivity, while not affecting the intensity of neuronal cell profiles. In the same vein, quantitative comparison of the area covered by CGRP^{+} sprouts (Fig. 7F) showed a 60% decrease in brain Jun-deficient animals compared with their *jun*$^{f/f}$ controls ($P < 2\%$, Student's *t*-test). Direct visual counting revealed a similar, approximately 67% decrease in the number of sprouts ($P < 5\%$).

Changes in beta1 integrin levels

The beta1 integrin subunit is the obligate partner of alpha7 and shows a neuronal expression peak 14 days following facial nerve cut (Kloss et al., 1999), so we next explored the relationship between sprouting response and levels of this regeneration associated molecule. As shown in Figure 8A, absence of the alpha7 integrin caused significantly elevated beta1 integrin levels at day 14 compared with littermate controls (+34%, $P < 5\%$, Student's *t*-test). Similarly, deletion of brain c-jun also showed a 68% decrease in beta1 integrin immunoreactivity following facial axotomy at day 14 (Fig. 8B; $P < 5\%$), in line with the absence in central sprouting observed in these mutants.

Figure 7. Effects of neural c-Jun (*jun*$^{\Delta N}$; **A–F**), TNFR1/2 (**G–I**), and alpha7 (**J–L**) gene deletions and LPS-induced inflammation (**M–R**) on galanin (A–C,G–R)-and CGRP (D–F)-immunoreactive central axonal sprouting in the facial motor nucleus 14 days after cut. Left row, littermate controls; center, mutants; right, quantification of the effects on the area (left Y-axis, parts per million) and number (#, right Y-axis) of galanin-or CGRP-positive sprouts (mean ± SEM, n = 3–6 animals per group). Solid bars, littermate controls; open bars, mutants. In the case of endotoxin (O), single intraperitoneal injection of 1 mg *E. coli* LPS /kg caused a transient decrease of sprouting 12–48 hours after injection (solid bars). Uninjected animals (0) and mice 24 hours after saline (sal) injection served as controls (open bars). *$P <$ 5%, Student's *t*-test (C,I) or ANOVA followed by post hoc Tukey test (O). The **inset** in F shows the overall CGRP immunoreactivity (in OLV values) in the axotomized (ax, solid bars) and contralateral (co, open bars) for the *jun*$^{f/f}$ controls (left) and *jun*$^{\Delta N}$ mutants (right). Scale bar = 200 μm in R (applies to A,C,G–R); 80 μm for D,E.

Administration of LPS did not affect beta1 integrin levels significantly at any of the time points (0.5–4 days) tested (Fig. 8D). There was also no significant difference between cut and crush injury at day 7 or day 14, but there was a 25% increase at day 10 (Fig. 8C). Reinjury paradigms (8 + 6, 14 + 8) caused a significant, 26% and 27% decrease ($P <$ 5%), respectively, compared with their controls at days 14 and 22 (Fig. 8E).

DISCUSSION

Regenerative axonal sprouting is critical for repair of the adult nervous system, but the specific signals involved are only beginning to be understood. The facial nerve axotomy model is a well-characterized paradigm for studying molecular mechanisms involved in successful peripheral regeneration and functional recovery, and previous studies have reported the appearance of central galanin^{+} sprouts inside the facial motor nucleus 14 days after nerve cut (Galiano et al., 2001; Makwana et al., 2007). The aim of the current set of experiments was to establish the neuroanatomical origin and distribution of these growth cone-carrying axons, determine the time course of their sprouting response, and identify physiological causes responsible for its transient appearance and regulation following injury.

As shown in the current study, transection of axons in the peripheral part of the facial motor nerve caused the delayed appearance of sprouting, galanin^{+}, and to a lesser extent CGRP^{+}, neurites inside the central nervous system, in and around the affected facial motor nucleus. These sprouts appeared to originate from axotomized facial motoneurons based on their selective appearance on the injured side; presence of vesicular acetylcholine transporter as a marker of cholinergic phenotype; presence of both galanin^{+} and CGRP^{+} subpopulations of facial motoneurons; and colocalization with the bidirectional, retrograde and anterograde, tracer Mini-Ruby first applied to the proximal stump of the cut facial nerve. As demonstrated in Figure 2H, cell body fluorescence for Mini-Ruby was completely limited to the axotomized facial motor nucleus. Together with the absence of axonal Mini-Ruby staining in sensory projection areas (brainstem, substantia gelatinosa, spinal nucleus of the trigeminal nerve), this argues against a major sensory contribution to the perifacial sprouting. This point is reinforced by the presence of VAChT as a marker of cholinergic phenotype on a large number, although not in all, of sprouts detected here and the fact that VAChT^{+} innervation of motoneurons is not affected by removal of sensory input (Oliveira et al., 2003). Finally, sprouts located outside the nucleus and visualized with their stalk and bulb had their leading structure, the growth cone bulb, in the majority of cases pointing away from the nucleus, suggesting growth away, not growth toward, the nucleus.

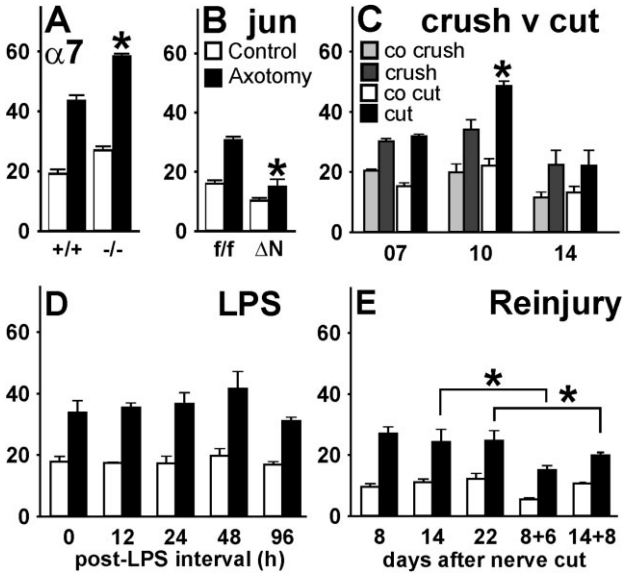

Figure 8. Effects of alpha7 (**A**) and neural *jun* (**B**) deletions, crush vs. cut (**C**), application of LPS (**D**), and additional nerve injury (**E**) on beta1 integrin subunit levels in the axotomized and contralateral facial motor nuclei. $*P < 5\%$, Student *t*-test (A–C) or ANOVA and post hoc Tukey test (E). Beta1 immunoreactivity was quantified by using the Mean-SD algorithm and is shown in OLV values, n = 3–6 animals per group, as in Figure 7. A,B,D show the results from facial motor nuclei 14 days after nerve cut; C compares crush with cut 7–14 days after axotomy; E shows the effects of second (cut) injury. co (C), contralateral side to the lesion.

Neurochemically, the detected sprouts clearly exhibited the profile of growing axon terminals. They contained high levels of anterogradely transported neuropeptides galanin and CGRP, synaptophysin, and VAChT; expressed regeneration-associated CD44 and alpha7beta1 integrin cell adhesion molecules (Werner et al., 2000; Raivich et al., 2004); and lacked MAP2, a typical component of dendritic cytoskeleton (McDermid et al., 2004). The absence of neurofilament H staining is also in line with the fact that neurofilaments do not extend into the terminal growth cone structures (Jacobs and Thomas, 1982; Tetzlaff and Bisby, 1989). Detailed morphological studies in similar models in axotomized cat spinal motoneurons and commissural interneurons showed that these sprouts had a long, axon-like process can project directly from the soma, proximal principal dendrite, or even very distal part of the dendrite, depending on the type of axotomized neuron (MacDermid et al., 2004; Fenrich et al., 2007). Although the current data focus more on the molecular characterization and regulatory dynamics of the sprouting response, it will be of considerable interest to identify in a future study the main subcellular origin of the prolific sprouting response that is observed following mouse facial axotomy.

Sprouting orientation

Theoretically, growth cones associated with the injured facial motor nucleus could be oriented in any direction with respect to the nucleus. In fact, they did show a clearly trimodal distribution (Fig. 1I), with three of the nine segments responsible for 70% of the orientations taken. Sprouts in the largest of these three groups (A, 38%) were oriented away from (0°–20°) and those in the smallest (I, 8%) were oriented directly toward the nucleus (160°–180°). Sprouts in the relatively large intermediate group (E, 24%) oriented themselves roughly perpendicular to the vector from the center of the nucleus and parallel (80–100°) to the outline of the nucleus proper. The overall predominance of outward-pointing sprouts appears to suggest the presence of a strong repellent cue associated with the injured facial motor nucleus, which would be consistent with the lower density of sprouts inside than directly outside the nucleus, as shown in Figure 1H. In the same vein, the presence of a smaller segment of sprouts pointing toward the nucleus (8% in I, 13% in the inward three segments G–I) could be due to a paradoxical reaction, reversing a repellent to an attractant response (Tear, 1998; Gavazzi, 2001) or the presence of bona fide attractors, to which only a smaller subpopulation is sensitive. Finally, instead of a gradual increase from the directly inward-to outward-pointing segments, there is a relatively large, intermediate fraction of "cruising" sprouts that run perpendicular to the vector from the nucleus center. Although at first puzzling, this could suggest that some sprouts lay a decidedly equidistant course between two similarly attractive directions.

At present the identity of signals regulating this orientation distribution are unknown. Injured facial motor neurons are known to change the expression for a series of chemorepellant molecules and their subcellular signalling, with increased semaphorin IIIC and plexin A2 synthesis (Pasterkamp et al., 1998; Spinelli et al., 2007; Oschipok et al., 2008). However, some repellent signals may also originate from neighboring microglia (Schifman and Selzer, 2007), which exhibit maximal activation at day 14 (Bohatschek et al., 2004), together with the peak sprouting response. Here, cell-type-selective deletion of expressed chemorepellent cues will improve insight into the cellular source and specific effects of signals guiding sprouting inside the adult central nervous system.

Effects of regeneration, reinnervation, and recut

The onset and peak of sprouting at day 7 and day 14 after cut occur at roughly the same time as the beginning of facial motoneuron reinnervation of their peripheral target described in previous studies (Werner et al., 2000; Raivich et al., 2004). Moreover, denervated muscle fibers

are a rich source of neutrophins and adhesion molecules (Covault and Sanes, 1985; Koliatsos et al., 1993; Funakoshi et al., 1993; Ishii et al., 1994; Springer et al., 1995) that could provide a transient surge in trophic signals available to axotomized motoneurons during the initial process of reconnection. However, our data do not suggest that reinnervation is responsible for the sudden burst in central axonal sprouting. Although reinnervation is known to occur earlier, more promptly, and with less error after crush than after cut (Nguyen et al., 2002; Witzel et al., 2005), peak levels of sprouting after cut were more than 5-fold higher than after crush. Similarly, the reinterruption of axonal connections with a recut (8 + 6, 14 + 8) led to a significantly stronger sprouting response compared with that observed following a single cut at day 14 and day 22, respectively. This enhanced sprouting could be due to a conditioning effect (Woolf et al., 1992; Gilad et al., 1996). However, the 14 + 8 sprouting was less than at day 14, suggesting that overall duration and presence of recut, rather than the conditioning effect, are the primary variables that define the extent of central sprouting.

Surprisingly, these facial axonal sprouts were particularly numerous in the white matter tissue that appears to inhibit the outgrowth of corticospinal, rubrospinal, or peripheral sensory axons via rapid growth cone collapse (Thallmair et al., 1998; McKerracher, 2001; Cafferty et al., 2008). At the ultrastructural level (Table 1), the facial sprouts showed frequent and close contact with neighboring myelinated sheaths (Fig. 6E, Table 1) and occasionally with the oligodendroglial cell bodies (Fig. 6A), while maintaining an active growth state. Interestingly, and unlike most of the cases mentioned above from previous studies, dissociated sensory neurons microtransplanted into the spinal cord showed almost no inhibition, growing robustly through normal or even through predegenerated white matter (Davies et al., 1999). In fact, they were stopped only by glial scars surrounding CNS lesions. Although these effects appeared to be specific for peripheral sensory neurons—similarly dissociated cortical neurons did not regenerate into white matter (Tom et al., 2004)—the facial sprouting response shown in the current study could suggest that similar resilience to white matter inhibitory signals is inducible in central neurons. Understanding the molecular signals associated with the formation of facial axonal sprouts could thus provide clues to improving regenerative response in the white matter of the central nervous system.

Neuronal cell death and inflammation

The peak in central axonal sprouting in the mouse facial axotomy model also coincides with the maximum in substantial neuronal cell death and also with inflammatory changes in microglia and astrocytes and leukocyte recruitment observed in this CNS injury and repair model. Previous evidence also shows that those subtypes of neurons that are most likely to be programmed to launch a regenerative response after injury, for example, retinal ganglion cells, also exhibit a high rate of cell death (Berkelaar et al., 1994), which is in line with observations in which particular transcription factors such as c-Jun that contribute to cell death are also required for regeneration (Raivich et al., 2004).

In the same vein, brain c-Jun-deficient animals with an absence of neuronal cell death following facial nerve cut (Raivich et al., 2004) do show a reduced sprouting response in the mutant animals. However, this correlation is not maintained in other mutants with effects on cell death in the same model. TNFR1/2 null mice show a 4-fold reduction in cell death (Raivich et al., 2002) and a slight, though not significant, tendency toward higher central sprouting. Transforming growth factor-β1 null mice also show greatly increased cell death, together with a significantly reduced sprouting response (Makwana et al., 2007). A similar lack of linear correlation is also observed for peripheral regeneration, with enhanced sprouting in IL6 null (Galiano et al., 2001) and alpha7 null (Fig 6G–I) animals and reduced sprouting in the brain c-jun-deficient animals (Fig 6A–F); all three groups of mutant mice show a significant reduction in the speed of peripheral nerve outgrowth (Zhong et al., 1999; Werner et al., 2000; Galiano et al., 2001; Raivich et al., 2004).

Current data do show a relatively straightforward correlation between neural inflammation and reduced central axonal sprouting in the facial axotomy model. Systemic application of 1 mg *E. coli* endotoxin causing severe neural inflammation and granulocyte recruitment (Bohatschek et al., 2001), resulted in a 50% reduction in sprouting response 12–48 hours following the intraperitoneal injection (Fig. 6M–R). Enhanced neural inflammation in TGF-beta1 null mice is associated with reduced sprouting (Makwana et al., 2007). This also appears to be true in reverse, with attenuated inflammation and 50% enhanced sprouting in IL6 null mice (Galiano et al., 2001). Finally, reduced inflammatory response in the TNFR1/2 null mice (Hristova et al., 2005; Bohatschek et al., 2005; Liu et al., 2006) coincides with the tendency toward improved sprout outgrowth in these mutant mice shown in the current study and agrees with the appearance of MAP2-negative dendraxon sprouts in permanently axotomized cat motoneurons (McDermid et al., 2004).

Induced inflammation around the cell body has been shown to improve sensory axon outgrowth into the CNS (Lu and Richardson, 1991). However, these results were obtained when inflammatory stimulus was used instead of peripheral nerve injury, unlike the current model in which peripheral injury is followed by a robust inflammatory re-

sponse inside the affected part of the brain (Moran and Graeber, 2004). Central injury frequently produces a mild retrograde reaction, in which additional inflammation will elicit a stimulatory effect (Hossain-Ibrahim et al., 2006), raising the question with regard to those components of neuronal response that specifically enhance neurite outgrowth inside the injured CNS.

Endogenous signals in central axonal sprouting

Up-regulation of neuronal transcription factors such as c-Jun, ATF3, or STAT3 plays an important role in the neural response to injury and the synthesis of molecules required for regeneration and repair (Herdegen and Leah, 1998; Tsujino et al., 2000; Schweizer et al., 2002). As shown in this study, neural expression of c-Jun transcription factor strongly supports the delayed appearance of central axonal sprouting. Although numerous regeneration-associated genes and proteins show an early onset and peak of expression following injury (e.g., ATF3, GAP43, CD44, CGRP, alpha7 integrin subunit) that may allow the different stages in the initiation and execution of neurite outgrowth (Seijffers et al., 2007), there is a second or later group of molecules such as galanin, beta1, and noxa (Kloss et al., 1999; Galiano et al., 2001; Kiryu-Seo et al., 2005; Di Giovanni et al., 2006) with a relatively delayed expression that coincides with central sprouting and neuronal cell death. Moreover, many of the late but also early molecules are brain c-Jun dependent and as shown in the current study are actually expressed in the facial axonal sprouts, for example, CD44, galanin, and alpha7beta1 integrin. These growth-cone-localized molecules support axonal elongation and outgrowth in the peripheral nerve (Werner et al., 2000; Holmes et al., 2000) and may enhance central sprouting as well as allow nascent central growth cones to withstand numerous inhibitory cues such as NOGO, MAG, and OMGP that are present in the white matter (McKerracher, 2001). Although hypothetical, the neurite-outgrowth enhancing properties of galanin could also be involved in the much stronger sprouting observed in the galanin$^+$ compared with the CGRP$^+$ populations of axotomized facial motoneurons.

Deletion of the alpha7 integrin subunit increases central sprouting, which could point to an inhibitory role of the alpha7beta1 integrin. Previous immunohistochemical studies revealed prominent localization of both integrin components, alpha7 and beta1, on the terminal parts of growing axons and the cell bodies of axotomized motor and sensory neurons, with very little expression on most of the axons or in dendritic arborizations (Kloss et al., 1999; Werner et al., 2000). The current study also shows a very similar distribution, with much higher levels of both components in the terminal part of the sprout than in the adjacent axon-like stalk (Fig. 5S–U,Z–AB,AC–AE), pointing to a specific growth cone function. Furthermore, the apparently compensatory up-regulation of beta1 could suggest enhanced activity, for example, via one of the other 11 currently identified beta1-associating alpha subunits (Sixt et al., 2006), by interacting with fibronectin, the main extracellular matrix component associated with the outgrowth of transplanted sensory neurons in central white matter, for example (Tom et al., 2004). Moreover, the strong decrease in posttraumatic neuronal expression of beta1 in brain Jun-deficient mice could also contribute to the reduction in central sprouting in these mutant animals.

This potential involvement of beta1-family integrins is qualified by incomplete overlap of peak beta1 levels (day 10) and sprouting (day 14) in the cut vs. crush experiment. It is possible that the regulatory control exerted by the alpha7beta1 integrin is in fact several steps upstream of the actual sprouting response, particularly inasmuch as the immunoreactivities for beta1 (Fig. 8C) and for alpha7 (Fig. 1b in Werner et al., 2000) both peak between day 7 and day 10 and are already strongly decreased at day 14. Moreover, the significant reduction of beta1 levels in the recut experiment was associated with enhanced sprouting (Fig. 7D,E) and could indicate the presence of additional pathways involved in the regulation of central axonal outgrowth under varying genetic and experimental conditions. Nevertheless, the hypothesis for beta1-integrin-family involvement will have to be tested using central neuronal deletion of the beta subunit to settle this issue. Furthermore, if these experiments do show positive involvement of beta1, identifying the cognate alpha subunit(s) involved in central axonal sprouting could enhance the therapeutic understanding of the repair processes operating in the injured brain and spinal cord.

ACKNOWLEDGMENTS

We gratefully acknowledge the help of Ms. Dietmute Büringer (Neuromorphology, Martinsried) and Mr. Mark Tully (Cell and Developmental Biology Department, UCL) for their expert assistance with electron microscopy and Prof. Horst Bluethmann (Hoffmann-LaRoche, Basel, Switzerland) for providing the TNFR1/2 null mice.

LITERATURE CITED

Behrens A, Sibilia M, David JP, Möhle-Steinlein U, Tronche F, Schütz G, Wagner EF. 2002. Impaired postnatal hepatocyte proliferation and liver regeneration in mice lacking c-jun in the liver. EMBO J 21:1782–1790.

Berkelaar M, Clarke DB, Wang YC, Bray GM, Aguayo AJ. 1994. Axotomy results in delayed death and apoptosis of retinal ganglion cells in adult rats. J Neurosci 14:4368–4374.

Blue ML, Davis G, Conrad P, Kelley K. 1993. Specific cleavage of the α4 integrin associated with activation of peripheral T lymphocytes. Immunol 78:80–85.

Bohatschek M, Werner A, Raivich G. 2001. Systemic LPS injection leads to granulocyte influx into normal and injured brain: effects of ICAM-1 deficiency. Exp Neurol 172:137–152.

Bohatschek M, Kloss CU, Hristova M, Pfeffer K, Raivich G. 2004. Microglial major histocompatibility complex glycoprotein-1 in the axotomized facial motor nucleus: regulation and role of tumor necrosis factor receptors 1 and 2. J Comp Neurol 470: 382–399.

Cafferty WB, McGee AW, Strittmatter SM. 2008. Axonal growth therapeutics: regeneration or sprouting or plasticity? Trends Neurosci 31: 215–220.

Covault J, Sanes JR. 1985. Neural cell adhesion molecule (N-CAM) accumulates in denervated and paralyzed skeletal muscles. Proc Natl Acad Sci U S A 82:4544–4548.

Cotman CW, Geddes JW, Kahle JS. 1990. Axon sprouting in the rodent and Alzheimer's disease brain: a reactivation of developmental mechanisms? Prog Brain Res 83:427–434.

Davies SJ, Goucher DR, Doller C, Silver J. 1999. Robust regeneration of adult sensory axons in degenerating white matter of the adult rat spinal cord. J Neurosci 19:5810–5822.

Di Giovanni S, Knights CD, Rao M, Yakovlev A, Beers J, Catania J, Avantaggiati ML, Faden AI. 2006. The tumor suppressor protein p53 is required for neurite outgrowth and axon regeneration. EMBO J 25:4084–4096.

Diamond J, Coughlin M, Macintyre L, Holmes M, Visheau B. 1987. Evidence that endogenous beta nerve growth factor is responsible for the collateral sprouting, but not the regeneration, of nociceptive axons in adult rats. Proc Natl Acad Sci U S A 84:6596–6600.

Echtermeyer F, Schöber S, Pöschl D, von der Mark H, von der Mark K. 1996. Specific induction of cell motility on laminin by 7 integrin. J Biol Chem 271:2071–2075.

Erickson SL, de Sauvage FJ, Kikly K, Carver-Moore K, Pitts-Meek S, Gillett N, Sheehan KC, Schreiber RD, Goeddel DV, Moore MW. 1994. Decreased sensitivity to tumour-necrosis factor but normal T-cell development in TNF receptor-2-deficient mice. Nature 372:560–563.

Fenrich KK, Skelton N, Macdermid VE, Meehan CF, Armstrong S, Neuber-Hess MS, Rose PK. 2007. Axonal regeneration and development of de novo axons from distal dendrites of adult feline commissural interneurons after a proximal axotomy. J Comp Neurol 502:1079–1097.

Friede RL, Bischhausen R. 1980. The fine structure of stumps of transected nerve fibers in subserial sections. J Neurol Sci 44:181–203.

Funakoshi H, Frisen J, Barbany G, Timmusk T, Zachrisson O, Verge VM, Persson H. 1993. Differential expression of mRNAs for neurotrophins and their receptors after axotomy of the sciatic nerve. J Cell Biol 123:455–465.

Galiano M, Liu ZQ, Kalla R, Bohatschek M, Koppius A, Gschwendtner A, Xu SL, Werner A, Kloss C, Bluethmann H, Raivich G. 2001. Interleukin-6 (IL6) and the cellular response following facial nerve injury: effects on lymphocyte recruitment, early microglial activation and axonal outgrowth in IL6-deficient mice. Eur J Neurosci 14:327–341.

Gavazzi I. 2001. Semaphorin-neuropilin-1 interactions in plasticity and regeneration of adult neurons. Cell Tissue Res 305: 275–284.

Gilad VH, Tetzlaff WG, Rabey JM, Gilad GM. 1996. Accelerated recovery following polyamines and aminoguanidine treatment after facial nerve injury in rats. Brain Res 724:141–144.

Gilmor ML, Nash NR, Roghani A, Edwards RH, Yi H, Hersch SM, Levey AI. 1996. Expression of the putative vesicular acetylcholine transporter in rat brain and localization in cholinergic synaptic vesicles. J Neurosci 16:2179–2190.

Harris J, Ayyub C, Shaw G. 1991. A molecular dissection of the carboxyterminal tails of the major neurofilament subunits NF-M and NF-H. J Neurosci Res 30:47–62.

Hemler ME, Crouse C, Takada Y, Sonnenberg A. 1988. Multiple very late antigen (VLA) heterodimers on platelets. Evidence for distinct VLA-2, VLA-5 (fibronectin receptor), and VLA-6 structures. J Biol Chem 263:7660–7665.

Herdegen T, Leah JD. 1998. Inducible and constitutive transcription factors in the mammalian nervous system: control of gene expression by Jun, Fos and Krox, and CREB/ATF proteins. Brain Res Rev 28:370–490.

Heumann R, Goemans C, Bartsch D, Lingenhohl K, Waldmeier PC, Hengerer B, Allegrini PR, Schellander K, Wagner EF, Arendt T, Kamdem RH, Obst-Pernberg K, Narz F, Wahle P, Berns H. 2000. Transgenic activation of Ras in neurons promotes hypertrophy and protects from lesion-induced degeneration. J Cell Biol 151:1537–1548.

Holmes FE, Mahoney S, King VR, Bacon A, Kerr NC, Pachnis V, Curtis R, Priestley JV, Wynick D. 2000. Targeted disruption of the galanin gene reduces the number of sensory neurons and their regenerative capacity. Proc Natl Acad Sci U S A 97: 11563–11568.

Holzmann B, Weissman IL. 1989. Integrin molecules involved in lymphocyte homing to Peyer's patches. Immunol Rev 108: 45–61.

Hossain-Ibrahim MK, Rezajooi K, MacNally JK, Mason MR, Lieberman AR, Anderson PN. 2006. Effects of lipopolysaccharide-induced inflammation on expression of growth-associated genes by corticospinal neurons. BMC Neurosci 7:8.

Hristova M, Cuthill D, Zbarsky V, Acosta-Saltos A, Wallace A, Blight K, Buckley SM, Peebles D, Heuer H, Waddington SN, Raivich G. 2009. Activation and deactivation of periventricular white matter phagocytes during postnatal mouse development. Glia 58:11–28.

Hu C, Mayadas-Norton T, Tanaka K, Chan J, Salgame P. 2000. Mycobacterium tuberculosis infection in complement receptor 3-deficient mice. J Immunol 165:2596–2602.

Ide C, Kato S. 1990. Peripheral nerve regeneration. Neurosci Res Suppl 13:S157–S164.

Ishii DN, Glazner GW, Pu SF. 1994. Role of insulin-like growth factors in peripheral nerve regeneration. Pharmacol Ther 62: 125–144.

Kalla R, Liu Z, Xu S, Koppius A, Imai Y, Kloss CU, Kohsaka S, Gschwendtner A, Möller JC, Werner A, Raivich G. 2001. Microglia and the early phase of immune surveillance in the axotomized facial motor nucleus: impaired microglial activation and lymphocyte recruitment but no effect on neuronal survival or axonal regeneration in macrophage-colony stimulating factor-deficient mice. J Comp Neurol 436:182–201.

King TE, Pawar SC, Majuta L, Sroka IC, Wynn D, et al. 2008. The role of $\alpha 6$ integrin in prostate cancer migration and bone pain in a novel xenograft model. PLoS ONE 3:e3535.

Kiryu-Seo S, Hirayama T, Kato R, Kiyama H. 2005. Noxa is a critical mediator of p53-dependent motor neuron death after nerve injury in adult mouse J Neurosci 25:1442–1447.

Kloss CUA, Werner A, Shen J, Klein MA, Kreutzberg GW, Raivich G. 1999. The integrin family of cell adhesion molecules in the injured brain: regulation and cellular localization in the normal and regenerating mouse facial nucleus. J Comp Neurol 441: 162–178.

Koliatsos VE, Clatterbuck RE, Winslow JW, Cayouette MH, Price DL. 1993. Evidence that brain-derived neurotrophic factor is a trophic factor for motor neurons in vivo. Neuron 10:359–367.

Li L, Zhou XF. 2001. Pericellular *Griffonia simplicifolia* I isolectin B4-binding ring structures in the dorsal root ganglia following peripheral nerve injury in rats. J Comp Neurol 439:259–274.

Linda H, Risling M, Cullheim S. 1985. "Dendraxons" in regenerating motoneurons in the cat: do dendrites generate new axons after central axotomy? Brain Res 358:329–333.

Liu BP, Cafferty WB, Budel SO, Strittmatter SM. 2006. Extracellular regulators of axonal growth in the adult central nervous system. Philos Trans R Soc Lond B Biol Sci 361:1593–1610.

Liu W, Hirata K, Kawabuchi M. 2005. The occurrence of nitric oxide synthase-containing axonal baskets surrounding large neurons in rat dorsal root ganglia after sciatic nerve ligation. Arch Histol Cytol 68:29–40.

Lu X, Richardson PM. 1991. Inflammation near the nerve cell body enhances axonal regeneration. J Neurosci 11:972–978.

MacDermid VE, Neuber-Hess MS, Rose PK. 2004. The temporal sequence of morphological and molecular changes in axotomized feline motoneurons leading to the formation of axons from the ends of dendrites. J Comp Neurol 468:233–250.

Makwana M, Jones LL, Cuthill D, Heuer H, Bohatschek M, Hristova M, Friedrichsen S, Ormsby I, Bueringer D, Koppius A, Bauer K, Doetschman T, Raivich G. 2007. Endogenous transforming growth factor beta1 suppresses inflammation and promotes survival in adult CNS. J Neurosci 27:11201–11213.

Mayer U, Saher G, Fässler R, Bornemann A, Echtermeyer F, von der Mark H, Miosge N, Pöschl E, von der Mark K. 1997. Absence of integrin alpha 7 causes a novel form of muscular dystrophy. Nat Genet 17:318–323.

McLachlan EM, Hu P. 1998. Axonal sprouts containing calcitonin gene-related peptide and substance P form pericellular baskets around large diameter neurons after sciatic nerve transection in the rat. Neuroscience 84:961–965

McLachlan EM, Janig W, Devor M, Michaelis M. 1993. Peripheral nerve injury triggers noradrenergic sprouting within dorsal root ganglia. Nature 363:543–546.

McKerracher L. 2001. Spinal cord repair: strategies to promote axon regeneration. Neurobiol Dis 8:11–18.

McQuarrie IG. 1985. Effect of conditioning lesion on axonal sprout formation at nodes of Ranvier. J Comp Neurol 231: 239–249.

Mehta A, Reynolds ML, Woolf CJ. 1993. Partial denervation of the medial gastrocnemius muscle results in growth-associated protein-43 immunoreactivity in sprouting axons and Schwann cells. Neuroscience 57:433–442.

Menon B, Krishnamurthy P, Kaverina E, Johnson JN, Ross RS, Singh M, Singh K. 2006. Expression of the cytoplasmic domain of beta-1 integrin induces apoptosis in adult rat ventricular myocytes (ARVM) via the involvement of caspase-8 and mitochondrial death pathway. Basic Res Cardiol 101:485–493.

Möller JC, Klein MA, Haas S, Jones LL, Kreutzberg GW, Raivich G. 1996. Regulation of thrombospondin in the regenerating mouse facial motor nucleus. Glia 17:121–132.

Moore RY. 1989. Cranial motor neurons contain either galanin-or calcitonin gene-related peptidelike immunoreactivity. J Comp Neurol 282:512–522.

Moran LB, Graeber MB. 2004. The facial nerve axotomy model. Brain Res Rev 44:154–178.

Nguyen QT, Sanes JR, Lichtman JW. 2002. Pre-existing pathways promote precise projection patterns. Nat Neurosci 5:861–867.

Oliveira AL, Hydling F, Olsson E, Shi T, Edwards RH, Fujiyama F, Kaneko T, Hökfelt T, Cullheim S, Meister B. 2003. Cellular localization of three vesicular glutamate transporter mRNAs and proteins in rat spinal cord and dorsal root ganglia. Synapse 50:117–129.

Oschipok LW, Teh J, McPhail LT, Tetzlaff W. 2008. Expression of Semaphorin3C in axotomized rodent facial and rubrospinal neurons. Neurosci Lett 434:113–118.

Pasterkamp RJ, Giger RJ, Verhaagen J. 1998. Regulation of semaphorin III/collapsin-1 gene expression during peripheral nerve regeneration. Exp Neurol 153:313–327.

Pinkstaff JK, Detterich J, Lynch G, Gall C. 1999. Integrin subunit gene expression is regionally differentiated in adult brain. J Neurosci 19:1541–1556.

Raivich G, Makwana M. 2007. The making of successful axonal regeneration: genes, molecules and signal transduction pathways. Brain Res Rev 53:287–311.

Raivich G, Reddington M, Haas CA, Kreutzberg GW. 1995. Peptides in motoneurons. Prog Brain Res 104:3–20.

Raivich G, Haas S, Werner A, Klein MA, Kloss C, Kreutzberg GW. 1998. Regulation of MCSF receptors on microglia in the normal and injured mouse central nervous system: a quantitative immunofluorescence study using confocal laser microscopy. J Comp Neurol 395:342–358.

Raivich G, Liu ZQ, Kloss CUA, Labow M, Bluethmann H, Bohatschek M. 2002. Cytotoxic potential of proinflammatory cytokines: combined deletion of TNF receptors TNFR1 and TNFR2 prevents motoneuron cell death after facial axotomy in adult mouse. Exp Neurol 178:186–193.

Raivich G, Bohatschek M, Clive DaCosta C, Iwata O, Galiano M, Hristova M, Wolfer DP, Lipp HP, Aguzzi A, Wagner EF, Behrens A. 2004. Essential role of the AP-1 transcription factor c-jun in axonal regeneration. Neuron 43:57–67.

Ramon y Cajal S. 1928. Degeneration and regeneration of the nervous system. London: Oxford University Press.

Rothe J, Lesslauer W, Lötscher H, Lang Y, Koebel P, Köntgen F, Althage A, Zinkernagel R, Steinmetz M, Bluethmann H. 1993. Mice lacking the tumour necrosis factor receptor 1 are resistant to TNF-mediated toxicity but highly susceptible to infection by *Listeria monocytogenes*. Nature 364:798–802.

Salmon AM, Damaj MI, Marubio LM, Epping-Jordan MP, Merlo-Pich E, Changeux JP. 2001. Altered neuroadaptation in opiate dependence and neurogenic inflammatory nociception in alpha CGRP-deficient mice. Nat Neurosci 4:357–358.

Schifman MI, Selzer ME. 2007. Differential expression of class 3 and 4 semaphorins and netrin in the lamprey spinal cord during regeneration. J Comp Neurol 501:631–646.

Schmits R, Filmus J, Gerwin N, Senaldi G, Kiefer F, Kundig T, Wakeham A, Shahinian A, Catzavelos C, Rak J, Furlonger C, Zakarian A, Simard JJ, Ohashi PS, Paige CJ, Gutierrez-Ramos JC, Mak TW. 1997. CD44 regulates hematopoietic progenitor distribution, granuloma formation, and tumorigenicity. Blood 90:2217–2233.

Schweizer U, Gunnersen J, Karch C, Wiese S, Holtmann B, Takeda K, Akira S, Sendtner M. 2002. Conditional gene ablation of Stat3 reveals differential signaling requirements for survival of motoneurons during development and after nerve injury in the adult. J Cell Biol 156:287–297.

Seijffers R, Mills CD, Woolf CJ. 2007. ATF3 increases the intrinsic growth state of DRG neurons to enhance peripheral nerve regeneration. J Neurosci 27:7911–7920.

Sigurjonsson OE, Perreault MC, Egeland T, Glover JC. 2005. Adult human hematopoietic stem cells produce neurons efficiently in the regenerating chicken embryo spinal cord. Proc Natl Acad Sci U S A 102:5227–5232.

Sixt M, Bauer M, Lammermann T, Fassler R. 2006. Beta1 integrins: zip codes and signaling relay for blood cells. Curr Opin Cell Biol 18:482–490.

Spinelli ED, McPhail LT, Oschipok LW, Teh J, Tetzlaff W. 2007. Class A plexin expression in axotomized rubrospinal and facial motoneurons. Neuroscience 144:1266–1277.

Springer JE, Seeburger JL, He J, Gabrea A, Blankenhorn EP, Bergman LW. 1995. cDNA sequence and differential mRNA regulation of two forms of glial cell line-derived neurotrophic factor in Schwann cells and rat skeletal muscle. Exp Neurol 131:47–52.

Tanigawa N, Saito T, Ogawa K, Iida H. 2005. Origin of regenerated axons in nerve bypass grafts. J Neurotrauma 22:605–612.

Tear G. 1998. Molecular cues that guide the development of neural connectivity. Essays Biochem 33:1–13.

Teixido J, Parkerlf CM, Kassner PD, Hemler ME. 1992. Functional and structural analysis of VLA-4 integrin $\alpha 4$ subunit cleavage. J Biol Chem 257:1786–1791.

Thallmair M, Metz GA, Z'Graggen WJ, Raineteau O, Kartje GL, Schwab ME. 1998. Neurite growth inhibitors restrict plasticity and functional recovery following corticospinal tract lesions. Nat Neurosci 1:124–131.

The UniProt Consortium. 2009. The Universal Protein Resource (UniProt). Nucleic Acids Res 37:D169–D174.

Tom VJ, Doller CM, Malouf AT, Silver J. 2004. Astrocyte-associated fibronectin is critical for axonal regeneration in adult white matter. J Neurosci 24:9282–9290.

Tronche F, Kellendonk C, Kretz O, Gass P, Anlag K, Orban PC, Bock R, Klein R, Schütz G. 1999. Disruption of the glucocorticoid receptor gene in the nervous system results in reduced anxiety. Nat Genet 23:99–103.

Tsujino H, Kondo E, Fukuoka T, Dai Y, Tokunaga A, Miki K, Yonenobu K, Ochi T, Noguchi K. 2000. Activating transcription factor 3 (ATF3) induction by axotomy in sensory and motoneurons: a novel neuronal marker of nerve injury. Mol Cell Neurosci 15:170–182.

Uhlenkott CE, Huijzer JC, Cardeiro DJ, Elstad CA, Meadows GG. 1996. Attachment, invasion, chemotaxis, and proteinase expression of B16-BL6 melanoma cells exhibiting a low metastatic phenotype after exposure to dietary restriction of tyrosine and phenylalanine. Clin Exp Metastasis 14:125–137.

von Ballestrem CG, Uniyal S, McCormick JI, Chau T, Singh B, Chan BM. 1996. VLA-beta 1 integrin subunit-specific monoclonal antibodies MB1.1 and MB1.2: binding to epitopes not dependent on thymocyte development or regulated by phorbol ester and divalent cations. Hybridoma 15:125–132.

Werner A, Willem M, Jones LL; Kreutzberg GW, Mayer U, Raivich G. 2000. Impaired axonal regeneration in a7-integrin deficient mice. J Neurosci 20:1822–1830.

Witzel C, Rohde C, Brushart TM. 2005. Pathway sampling by regenerating peripheral axons. J Comp Neurol 485:183–190.

Woolf CJ, Shortland P, Coggeshall RE. 1992. Peripheral nerve injury triggers central sprouting of myelinated afferents. Nature 355:75–78.

Zhong J, Dietzel ID, Wahle P, Kopf M, Heumann R. 1999. Sensory impairments and delayed regeneration of sensory axons in interleukin-6-deficient mice. J Neurosci 19:4305–4313.